Geophys. J. Int. (1997) **131**, 643–666

The time-averaged geomagnetic field: global and regional biases for 0–5 Ma

Catherine L. Johnson[1] and Catherine G. Constable[2]

[1] *Department of Terrestrial Magnetism, Carnegie Institution of Washington, 5241 Broad Branch Road, N.W. Washington,* DC 20015, *USA*
[2] *Institute for Geophysics and Planetary Physics, Scripps Institution of Oceanography, La Jolla,* CA 92093-0225, *USA*

Accepted 1997 June 27. Received 1997 June 12; in original form 1997 January 21

SUMMARY

Palaeodirectional data from lava flows and marine sediments provide information about the long-term structure and variability in the geomagnetic field. We present a detailed analysis of the internal consistency and reliability of global compilations of sediment and lava-flow data. Time-averaged field models are constructed for normal and reverse polarity periods for the past 5 Ma, using the combined data sets. Non-zonal models are required to satisfy the lava-flow data, but not those from sediments alone. This is in part because the sediment data are much noisier than those from lavas, but is also a consequence of the site distributions and the way that inclination data sample the geomagnetic field generated in the Earth's core. Different average field configurations for normal and reverse polarity periods are consistent with the palaeomagnetic directions; however, the differences are insignificant relative to the uncertainty in the average field models. Thus previous inferences of non-antipodal normal and reverse polarity field geometries will need to be re-examined using recently collected high-quality palaeomagnetic data. Our new models indicate that current global sediment and lava-flow data sets combined do not permit the unambiguous detection of northern hemisphere flux lobes in the 0–5 Ma time-averaged field, highlighting the need for the collection of additional high-latitude palaeomagnetic data. Anomalous time-averaged field structure is seen in the Pacific hemisphere centred just south of Hawaii. The location of the anomaly coincides with heterogeneities in the lower mantle inferred from seismological data. The seismic observations can be partly explained by lateral temperature variations; however, they also suggest the presence of lateral compositional variations and/or the presence of partial melt. The role of such heterogeneities in influencing the geomagnetic field observed at the Earth's surface remains an unresolved issue, requiring higher-resolution time-averaged geomagnetic field models, along with the integration of future results from seismology, mineral physics and numerical simulations.

Key words: core–mantle boundary, geomagnetism, palaeomagnetism, secular variation, time-averaged field.

1 INTRODUCTION

It is well known that, to a first-order approximation, the time-averaged direction of the geomagnetic field at any point on Earth is that due to a geocentric axial dipole, oriented either in its current (normal) or in the antipodal (reverse) direction, and that the field spends comparatively little time in transition between the stable polarity normal and reverse states. Less well known is the nature of the second-order contributions to the field; the largest is described in spherical harmonic models by a geocentric axial quadrupole, but its magnitude and those of other non-axial-dipole contributions to the field are poorly determined. Quantifying such second-order structure in the time-averaged geomagnetic field is critical, not only to our understanding of geodynamo processes, but also to understanding the influence of long-term boundary conditions (at either the inner core or outer core boundary) on flow in the outer core. Thermal and/or compositional variations at the base of the lower mantle have been inferred from velocity anomalies observed in global (and regional) seismic tomographic models (Clayton & Comer 1983; Dziewonski 1984; Hager & Clayton 1989; Innoue *et al.* 1990; Woodward &

Masters 1991; Masters & Bolton 1991; Morelli & Dziewonski 1991; Masters, Bolton & Shearer 1992; Pulliam, Vasco & Johnson 1993; Su, Woodward & Dziewonski 1994; Vasco *et al.* 1994, 1995; Li & Romanowicz 1996; Masters *et al.* 1996; Bolton 1996; van der Hilst, Widiyantoro & Engdahl 1997; review in Dziewonski 1996). It is possible that long-lived heterogeneities in the physical properties of the lower mantle influence convective flow patterns in the top of the outer core (e.g. Bloxham & Gubbins 1985; Gubbins & Richards 1986) and, in turn, the structure of the time-averaged geomagnetic field (Merrill & McElhinny 1977; Gubbins 1988; Merrill, McFadden & McElhinny 1990). There is increasing agreement on both amplitudes and wavelengths of lower-mantle seismic velocity anomalies, but inferences of a thermal or compositional origin for these anomalies are still under debate (see review by Loper & Lay 1995). Although considerable progress has been made on numerical dynamo simulations during the past few years (Glatzmaier & Roberts 1995a,b; Jones 1996; Kuang & Bloxham 1995, 1996), models for assessing the importance of thermal, topographic or electromagnetic core–mantle coupling on flow in the outer core are still a long way from accurate representation of the real Earth (Bloxham & Jackson 1990; Olson & Glatzmaier 1996; Zhang & Gubbins 1992, 1993). In this paper, we focus on whether detectable long-term lateral heterogeneities persist in the geomagnetic field, using palaeomagnetic data spanning the last 5 Myr (0–5 Ma).

The lack of knowledge of the detailed time-averaged field structure stems in part from the limited spatial and temporal distribution of palaeomagnetic data. Another problem is that there is no definitive time interval that one can say is required to define an average state for the field. It is not even known if the second-order terms do converge to any kind of stable average value. A related, but distinct, question is whether there are intrinsic differences between normal and reverse polarity states. During the last decade, significant effort has gone into compiling palaeomagnetic data sets from lava flows (Quidelleur *et al.* 1994; Johnson & Constable 1996; McElhinny, McFadden & Merrill 1996a; McElhinny & McFadden 1997) and sediments (Schneider & Kent 1988, 1990; McElhinny *et al.* 1996a; McElhinny & McFadden 1997), and these have been used to construct models of the time-averaged magnetic field. These data sets, and models of the time-averaged field derived from them, all indicate differences between the normal and reverse polarity average field geometry over the last few million years, but the source of the differences remains unclear. Potential candidates are rock magnetic noise, inadequate temporal and spatial sampling within each polarity epoch, and the possibility that there is no average stable polarity configuration for the geomagnetic field over timescales as short as a few million years. Genuine differences in average normal and reverse polarity stable field configurations also remain a possibility, but are hard to justify on theoretical grounds.

Another unresolved question is the nature of any non-zonal (longitudinally varying) contribution to the average field. Tantalizing evidence has accumulated regarding the tendency of geomagnetic reversal records to produce virtual geomagnetic pole (VGP) paths that track within a longitudinal band over the Americas and its antipode (Clement 1991; Laj *et al.* 1991), although interpretation of these data is controversial (Valet *et al.* 1992; Prévot & Camps 1993). In historical field models extending from 1980 back to 1690 it has been noted that there is low secular variation and minimal westward drift in the Pacific Hemisphere; the region is bounded by the longitudes of large flux lobes that appear at high latitudes and are especially distinct in the Northern Hemisphere (see review in Bloxham, Gubbins & Jackson 1989). This has led to speculation that there may be differences in structure beneath the Pacific Hemisphere near the core–mantle boundary (CMB) that are reflected in the behaviour of the time-averaged field (TAF) (Laj *et al.* 1991; Runcorn 1992). More recently it has been argued that VGPs may track in different bands for each reversal, indicating a possibility of shorter time-constant controls exerted by the inner core on field structure (Clement & Stixrude 1995). Hemispheric differences in the TAF, if they exist, should be manifest in palaeomagnetic data from stable polarity intervals, which are generally more reliable, as well as more numerous, than those from times when the field is reversing. However, although recent models point to the existence of non-zonal (or longitudinal) effects (Gubbins & Kelly 1993; Johnson & Constable 1995; Kelly & Gubbins 1997), it has so far proved difficult to say anything definitive about their form.

We revisit data sets from sediments compiled by Schneider & Kent (1988, 1990) and from lavas by Johnson & Constable (1995, 1996). We assess the regional consistency within the individual data sets, and determine appropriate uncertainty levels for data averaged within 5° spatial bins. By exploring how different types and distributions of data sample the field from the Earth's core, we show that inclination data available from marine sediments are unable to detect non-zonal structure in the geomagnetic field. However, when the sediment data are combined with the directions from lava flows, the sampling of the core–mantle boundary is much improved. We examine three subsets of the data—Brunhes epoch, 0–5 Ma normal and 0–5 Ma reverse data—and demonstrate that zonal models are inadequate to describe the time-averaged field structure observed in the data. Detailed analysis of inversions for non-zonal structure indicate that computed data uncertainties need to be increased by approximately 10–30 per cent in order to obtain models in which the spatial structure is robust. Time-averaged field models for 0–5 Ma normal and reverse polarity data are presented, along with jackknife estimates of the uncertainty in the models. The non-axial dipole structure in these models is compared with other recent inversions for the time-averaged field structure. Differences between normal and reverse polarity fields are examined and their significance evaluated relative to uncertainties in the models. Non-zonal structure in the models, in particular in the Pacific Hemisphere, is compared with seismological observations of CMB structure. Implications for long-term boundary conditions on outer core flow are discussed briefly in the light of our new results (see also Johnson & Constable 1997).

2 THE GLOBAL TIME-AVERAGED GEOMAGNETIC FIELD

It is commonly agreed that first-order structure in the time-averaged field can be described by a geocentric axial dipole (GAD). Deviations from this field are often reported as inclination or declination anomalies, defined as the observed inclination or declination at a particular site minus that predicted at the site location by a geocentric axial dipole field. These anomalies indicate the magnitude of any second-order signal in the observations. To model second-order contributions

to the TAF, we adopt the conventional spherical harmonic representation for the geomagnetic field: the magnetic scalar potential in the source free region due to an internal field generated in the Earth's core is

$$\Psi(r,\theta,\phi) = r_a \sum_{l=1}^{\infty} \sum_{m=0}^{l} \left(\frac{r_a}{r}\right)^{l+1} \times (g_l^m \cos m\phi + h_l^m \sin m\phi) P_l^m(\cos\theta), \quad (1)$$

where g_l^m and h_l^m are the Schmidt partially normalized Gauss coefficients, r_a is the radius of the Earth, r, θ and ϕ are radius, latitude and longitude, respectively, and P_l^m are the partially normalized Schmidt functions. The magnetic field, **B**, is the gradient of the potential Ψ, and a field model is specified by the Gauss coefficients g_l^m, h_l^m. The $m = 0$ terms in the expansion of eq. (1) correspond to spherical harmonic functions with no azimuthal structure, i.e. they are axially symmetric or zonal. g_1^0, g_2^0 and g_3^0 are known as the axial dipole, axial quadrupole and axial octupole terms, respectively.

This paper uses the field directions most often measured in palaeomagnetic work, namely the inclination (I) and declination (D),

$$D = \tan^{-1}\left(\frac{Y}{X}\right), \qquad I = \tan^{-1}\left(\frac{Z}{(X^2+Y^2)^{1/2}}\right). \quad (2)$$

X, Y and Z are, respectively, the north, east and downward pointing, locally orthogonal magnetic field components. For an axisymmetric field geometry Y, and hence declination, are identically zero, and inclination is a function only of latitude.

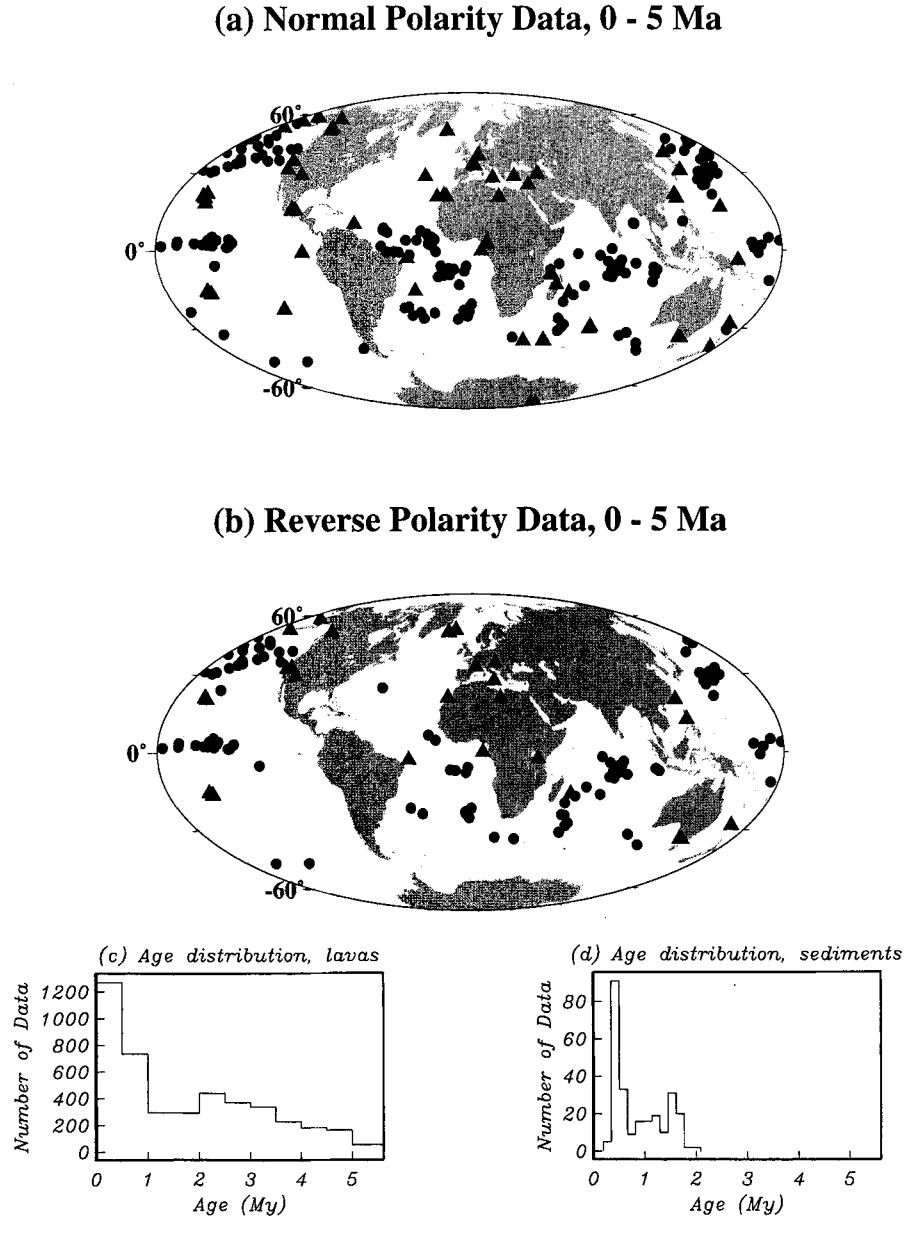

Figure 1. Spatial and temporal distribution of data sets used in this study. (a) Normal and (b) reverse polarity sediment core (circles; Schneider & Kent 1990) and lava-flow sequence (triangles; Johnson & Constable 1995, 1996) locations. (c) Age distribution of lava-flow data—normal and reverse combined (as in JC95, Fig. 2). Data from each location are assumed to be uniformly distributed over the age interval quoted. (d) Age distribution of sediment data—mean age for each core is given in database (Schneider & Kent 1990).

We use Occam's inversion (Constable, Parker & Constable 1987; Parker 1994) to construct regularized models of the TAF from time-averaged declination and inclination observations. The specific application of the algorithm to palaeomagnetic data from lava flows is described by Johnson & Constable (1995). Others have used this (Carlut & Courtillot 1997) or similar (Gubbins & Kelly 1993; Kelly & Gubbins 1997) techniques in palaeofield modelling. Regularized geomagnetic field models have minimum structure compatible with fitting the observations to a specified tolerance level. The penalty on structure used for the models presented here minimizes the root-mean-square (RMS) value of the radial magnetic field at the core–mantle boundary. We discuss the effects of other, more severe structure constraints. Because we are interested in the core field we plot our field models at the surface of the Earth's core. Regularized inversions have been used to construct minimum structure models for historical data (see e.g. Bloxham *et al.* 1989); thus the application of this technique to palaeomagnetic data allows direct comparison of average historical and palaeofield structures.

3 DATA

The spatial and temporal distributions of lava flows and piston sediment cores suitable for modelling the TAF over the past 5 Myr are shown in Fig. 1. Lava-flow data (Johnson & Constable 1996) alone require non-zonal structure in the TAF (Johnson & Constable 1995), in contrast to sediment data alone (Schneider & Kent 1988, 1990; this paper). Although a previous study (Gubbins & Kelly 1993; Kelly & Gubbins 1997) has used both lava-flow and sediment data in inversions for the TAF, a detailed investigation of the effect of data quality, distribution and type was not performed. Of particular interest is whether the non-zonal structure, in models compatible with the lava-flow data, is a reliable representation of the TAF. Both declination and inclination measurements are available from lava-flow data, whereas we have only inclination data for the sediment cores (a limitation we discuss further in the next section). In this section we review the internal consistency of each data set so that we can assign appropriate uncertainties to the data in the inversion procedure.

3.1 Lava flows

The lava-flow set has been described in some detail by Johnson & Constable (1996) and used in an earlier paper (Johnson & Constable 1995; hereafter JC95) to generate models of the TAF for the Brunhes, the normal polarity field for the time period 0–5 Ma, and the reverse polarity field for 0–5 Ma. The data set consists of directions measured from 2187 flows, 1528 of which are normal and 659 of which are reversed. Directions at each location are averaged to provide a sample of the time-averaged field, and an estimate of the directional uncertainty due to secular variation and rock magnetic and orientation error is made using the standard error in the averaged data. (Note that it is not necessary to combine the standard error with an estimate of the 'within-site' error, as was done incorrectly in JC95, Appendix A, since the standard error in the averaged data includes the effect of both secular variation and orientation error. Thus the uncertainties assigned to the lava-flow data in this paper are slightly lower than those in JC95. In the absence of any other modifications to the data and modelling procedure, this decrease in the estimates of data uncertainties results in models which fit the data and are similar to models LB1, LN1, LR1 in JC95 but in which some short-wavelength features are enhanced in amplitude relative to their counterparts in LB1, LN1 and LR1.) The data are summarized in Table 1 of JC95; there are 34 distinct sites for the Brunhes, 79 for all 0–5 Ma normal polarity and 34 for 0–5 Ma reversed polarity. Fig. 2 shows the time-averaged inclination anomaly as a function of site latitude, for the normal and reverse locations separately. The inclination anomaly is predominantly negative for normal polarities and positive for reverse polarities, reflecting the well-known far-sided effect (Wilson 1970). The non-zonal signal in the lava flows is better assessed using global maps of the inclination and declination anomalies, and is described in detail in JC95. Figs 3(b) and (c) show those for the normal polarity field, and Figs 4(b) and (c) show those for reversed polarity.

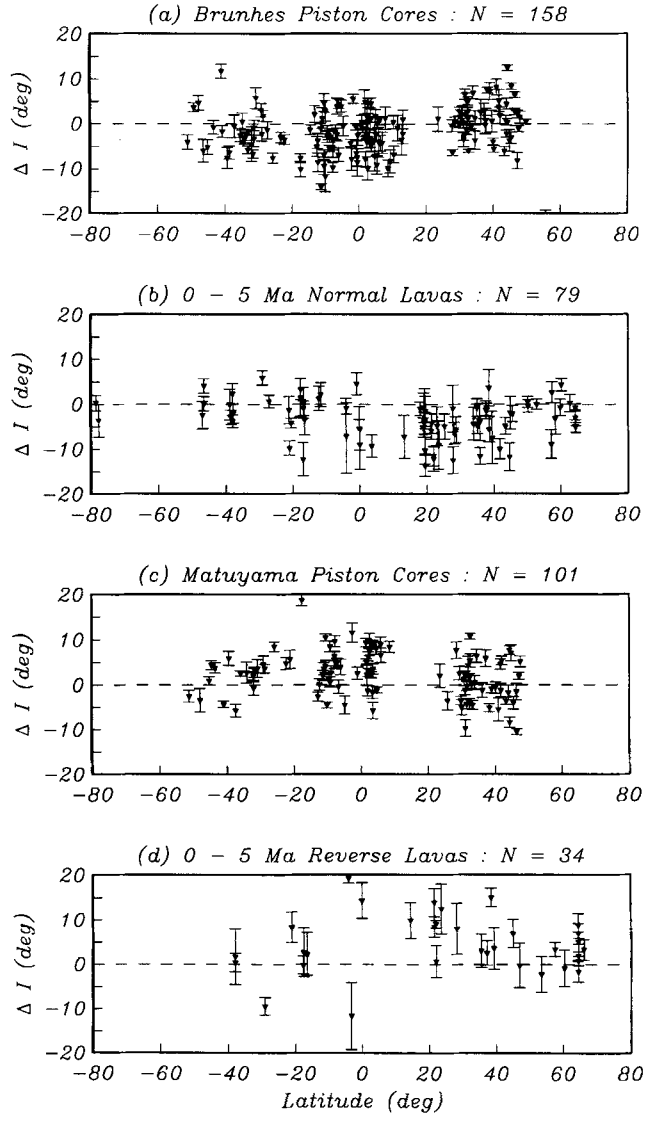

Figure 2. Inclination anomalies as a function of latitude for (a) Brunhes sediments, (b) normal polarity lavas, (c) Matuyama sediments, (d) reverse lavas. Triangles denote the mean inclination anomaly for each sediment core or sequence of flows at a given location; error bars are the standard error in the anomaly. N is the number of cores or lava-flow locations for each subset of data.

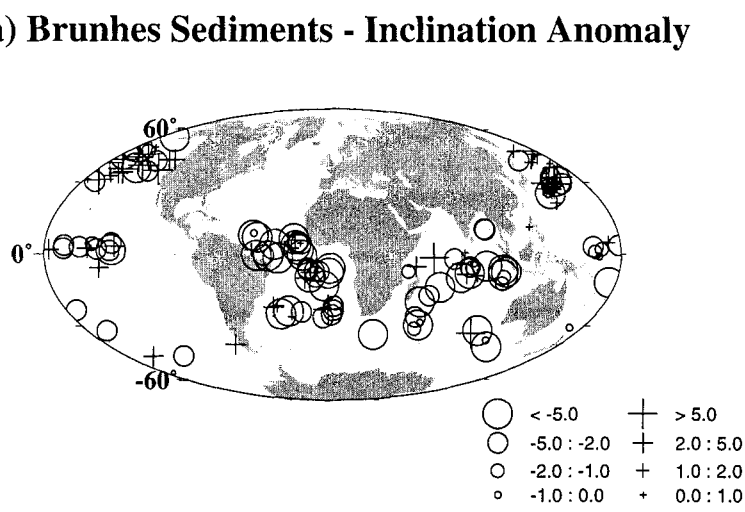

Figure 3. Inclination anomalies for (a) Brunhes sediments, and (b) normal lavas, and declination anomalies for (c) normal lavas. Negative anomalies are denoted by circles, positive anomalies by plus signs; the size of the sign corresponds to the magnitude of the anomaly in degrees as indicated by the legend.

Again, the far-sided effect in the inclination anomalies is evident. The declination anomalies are less consistent than the inclination anomalies: there are larger uncertainties associated with declination data, and furthermore the intrinsically greater range of variability than in inclination means they are more strongly affected by inadequate temporal sampling. Prior to computing TAF models, the 0–5 Ma data sets were averaged within 5° spatial bins: this improves the temporal sampling in some cases, and gives a more realistic estimate of the uncertainty to be expected from secular variation. In particular, after spatial averaging, the non-zonal structure in the declination measurements for the normal polarity data is much clearer. On average, small (positive) declination anomalies are seen through western North America and the southeast Pacific, and similarly small positive anomalies are observed through Europe and Africa. Large negative anomalies are found in the North and South Atlantic and in the western Pacific. Modelling demonstrates that non-zonal structure is present in the inclination anomalies for both the normal and reverse data (Section 8); however, this structure is not obvious in the crude visual representations of the raw data in Figs 2–4. After averaging, the numbers of normal and reverse polarity locations are reduced to 39 and

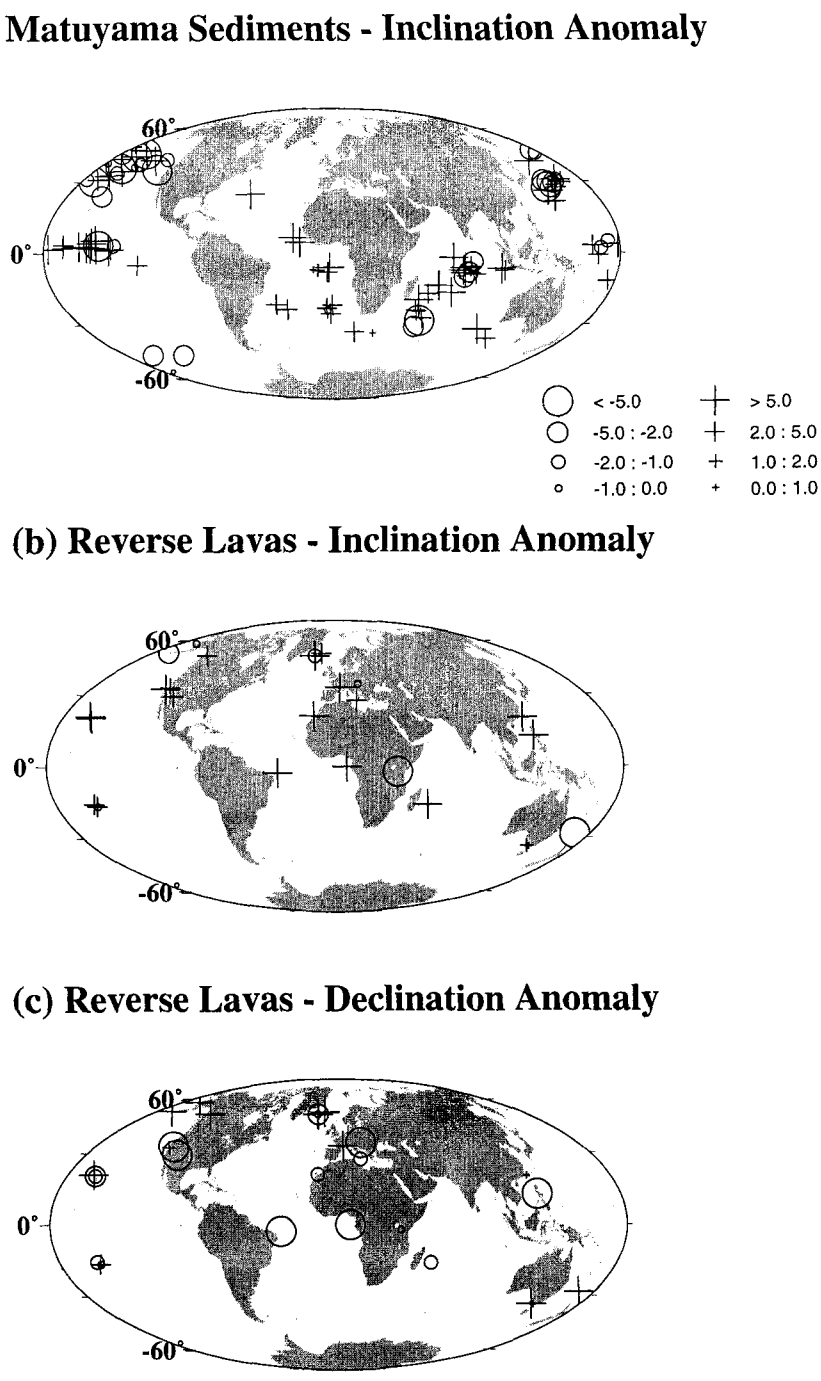

Figure 4. Inclination anomalies for (a) Matuyama sediments, and (b) reverse lavas, and declination anomalies for (c) reverse lavas. Figure format is as in Fig. 3.

22, respectively. The data set used for the Brunhes models was treated differently because of the small number of sites (see JC95): combining data from two nearby Hawaiian and two North American locations reduced the number of data points to 32. Additional inspection of the three data subsets led to the elimination of a further 1, 6 and 2 data points from the 0–5 Ma reverse, 0–5 Ma normal and Brunhes period data sets, respectively (Table 1), on the basis of less reliable temporal sampling, and one or more of (1) small number of flows, (2) regionally inconsistent declination or inclination anomalies, and (3) possible inadequate demagnetization.

3.2 Sediments

The piston core sediment data are concentrated in low–mid latitudes, with a dearth of samples in the North Atlantic (Fig. 1). The original database (Schneider & Kent 1990; hereafter SK90) contains 176 cores with Brunhes data and 125 cores with Matuyama data. For consistency with our lava-flow data (Johnson & Constable 1996), we removed sediment cores with a value of the precision parameter, k, less than 30, leaving 158 Brunhes and 101 Matuyama cores. Cores were averaged spatially in 5° bins to improve regional consistency,

Table 1. Data removed from lava-flow data set.

Location	λ	ϕ	N	ΔI	Polarity	*Reasons Data Removed*
Turkey	39	29	5	-3.7	N	low demag levels, low N, possible temporal undersampling
Turkey	40	44	5	-7.4	N	low demag levels, low N, anomalously large ΔI
Fernando de Noronha	-4	-32	7	-0.9	N	low N, regionally inconsistent ΔI due to 1 flow
New Guinea	-4	150	5	-6.9	B/N	low N, no details on demagnetization
Trinidade	-21	-29	5	-4.2	N	low N, possible temporal undersampling
Libya	28	173	10	-12.4	B/N	possibly only sampled early Brunhes, inconsistent ΔI
Fernando de Noronha	-4	-32	5	19.3	R	low N, 1967 reference, poor demag, regionally inconsistent ΔI

Location is given by latitude λ, and longitude ϕ. N is the number of flows sampled; ΔI is the inclination anomaly; polarity refers to the subset of data from which site removed (B = Brunhes; N = 0–5 Ma normal; R = 0–5 Ma reverse). The last column lists the main reasons for the data being removed, in addition to the incompatibility of data observed during global field modelling.

resulting in 116 Brunhes data and 75 Matuyama data. Fig. 2 shows the (unbinned) inclination anomalies as a function of latitude. The latitudinal variation is similar in shape to that seen in the lava flows, but is slightly diminished in intensity. The anomalies are dominantly negative during the Brunhes and positive during the Matuyama; however, there appears to be a slight positive bias for normal data (and negative bias for reverse data) at mid–northerly latitudes that is not seen in the flow data. The standard error in inclination for each core (from Schneider & Kent 1988, 1990) is typically of the order of 1°; however, as can be seen in Figs 3(a) and 4(a), this does not reflect the strong regional variability in inclination estimates. For lava-flow data this variability might be caused by inadequate temporal sampling at one or more sites; however, sediment cores should provide a good time-averaged field direction because the record is almost continuous and a large number of sample directions are averaged to give an inclination anomaly for each core. Regional variability in inclination anomalies recorded by sediments therefore suggests inconsistency among the observations; this can be caused by inadequate demagnetization of some cores and by non-vertical coring, which are not taken into account in the standard errors plotted in Fig. 2. Cores from the North Pacific region appear to be particularly inconsistent—these cores were some of the first piston cores to be collected and were only AF demagnetized at 5–15 mT compared with 15–40 mT for some later cores (SK90). There is therefore the possibility of residual contamination of the signal by viscous remanent magnetization.

We experimented with a variety of methods to obtain improved estimates of the uncertainty in the sediment inclination observations, all of which were based on assessing the regional consistency of the observed signal. Initially we used spherical splines (Parker 1994) to provide regional estimates of inclination compatible with the data. The difference between the inclination recorded by a particular core and the regional estimate of inclination provided an improved estimate of the uncertainty associated with the inclination measurement. However, the choice of appropriate spherical spline model was somewhat ad hoc and so we ultimately resorted to a simpler method. We assigned the cores to geographic clusters (approximately 20° bins), computed the average inclination anomaly for the cluster, and estimated the standard deviation in the distribution of anomalies about the mean value. From this we concluded that inclination anomalies at low latitudes and mid-southern latitudes were somewhat better detemined than those from elsewhere (North Pacific and high southern latitudes). On the basis of this analysis, we assigned inclination anomalies from cores in the latitude band 15°N–30°S a standard error of 4°, and those from higher latitudes a standard error of 5°. Experimentation showed that the modelling results of Section 8 are not very sensitive to the details of how we estimate these uncertainties; however, it is important to get a reasonable estimate of the size of the average uncertainty of the sediments relative to the lava-flow observations, to ensure that the sediments do not strongly outweigh the lava flows in the inversion procedure.

4 SAMPLING THE CORE–MANTLE BOUNDARY

Differences in the type and spatial distribution of data from flows and sediments affect the resulting field models. Eq. (1) gives the solution of Laplace's equation in terms of spherical harmonic functions, and for a particular set of spherical harmonic coefficients allows the calculation of the resulting potential or associated magnetic field at any point outside the assumed source region in the Earth's core. An alternative way of writing the magnetic field at the Earth's surface is in terms of the Green's function for $B_r(\hat{s})$, the radial magnetic field at the core–mantle boundary (CMB):

$$\mathbf{B}(\mathbf{r}) = \int_S \mathbf{G}(\mathbf{r}|\hat{\mathbf{s}}) B_r(\hat{s})\, d^2\hat{s}. \tag{3}$$

The justification for this is the uniqueness theorem for the solution of the exterior form of the Neumann boundary value problem for Laplace's equation (Mikhlin 1970, p. 270), and the form of the Green's functions has been published a number of times in the geomagnetic literature (see e.g. Gubbins & Roberts 1983; Constable, Parker & Stark 1993). We repeat them here for convenience:

$$\begin{aligned} G_X &= -\frac{(1+2R-\rho^2)}{R^3 T}\rho^3 \hat{s}\cdot\hat{x}, \\ G_Y &= -\frac{(1+2R-\rho^2)}{R^3 T}\rho^3 \hat{s}\cdot\hat{y}, \\ G_Z &= \rho^2 - \frac{\rho^2(1-\rho^2)}{R^3}, \end{aligned} \tag{4}$$

where we have $\rho = c/a$, $R = \sqrt{1-2\mu\rho+\rho^2}$, $\mu = \cos\alpha = \hat{r}\cdot\hat{s}$, and $T = 1 + R - \mu\rho$.

The components of $\mathbf{G} = (G_X, G_Y, G_Z)$ indicate the influence

$B_r(\hat{s})$ has on the local orthogonal components of the geomagnetic field at the Earth's surface. The Z component of the field is most sensitive to sources directly below the observation site (differentiating G_Z with respect to α gives $\alpha = 0°$ when $\partial G_Z/\partial\alpha = 0$), while the maximum contribution to the X and Y components is from sources located 23° away (differentiating G_X and G_Y with respect to α). Palaeomagnetic data rarely provide complete vector field information; the lava-flow data used here are declination and inclination measurements, and the sediment data are inclination alone. Declination and inclination are non-linear functionals of $B_r(\hat{s})$, but we can write equations that show how D and I respond to changes in $B_r(\hat{s})$. Suppose that $B_r(\hat{s})$ takes on the value of B_c at some point $\hat{s}_i$ on the CMB. Then we can evaluate the change in D or I measured at position $\mathbf{r}$ due to a change in B_c using

$$\begin{aligned}\frac{\partial D(\mathbf{r})}{\partial B_c(\hat{s}_i)} &= \frac{1}{H^2(\mathbf{r})}\left[X(\mathbf{r})\frac{\partial Y(\mathbf{r})}{\partial B_c} - Y(\mathbf{r})\frac{\partial X(\mathbf{r})}{\partial B_c}\right] \\ &= \frac{1}{H^2(\mathbf{r})}[X(\mathbf{r})G_Y(\mathbf{r}|\hat{s}_i) - Y(\mathbf{r})G_X(\mathbf{r}|\hat{s}_i)] \\ &= G_D,\end{aligned} \tag{5}$$

and similarly

$$\begin{aligned}\frac{\partial I(\mathbf{r})}{\partial B_c(\hat{s}_i)} &= \frac{1}{H^2 + Z^2}\left[HG_Z - \frac{Z}{H}(XG_X + YG_Y)\right] \\ &= G_I.\end{aligned} \tag{6}$$

These data kernels can be used to indicate the response of D and I to departures from an axial dipole field configuration, by linearizing about the response the dominantly axial dipole field values for X, Y, Z and H, i.e. substituting $Y = 0$, $X = \sin\theta$, etc. in the above. We call these linearized data kernels $G_{D_{ad}}$ and $G_{I_{ad}}$ for declination and inclination, respectively. Unlike the kernels for X, Y, and Z, the declination and inclination kernels vary with geographic location. Fig. 5 shows $G_{D_{ad}}$ and $G_{I_{ad}}$ at the CMB for surface observation points at latitudes of 0°, 30° and 60°N. These show the contribution of the core field, $B_r(\hat{s})$, to D and I anomalies at various latitudes, and demonstrate that models built from inclination data alone are not much influenced by $B_r(\hat{s})$ at high latitudes or at longitudes distant from the sample site. The declination sampling is somewhat complementary to that of the inclination, with little contribution from $B_r(\hat{s})$ immediately under the site, but covering a substantial longitudinal range.

We use the declination and inclination kernels to give an idea of how well our data sets sample the CMB in looking for departures from a geocentric axial dipole field. At each point, $\hat{s}$, on the CMB we sum the magnitudes of the contributions from $G_{D_{ad}}$ and $G_{I_{ad}}$ for the available sampling sites $\mathbf{r}_i$, $i = 1, \ldots, N$. We define the sampling function

$$S(\hat{s}) = \sum_i^N |G_{D_{ad}(\mathbf{r}_i|\hat{s})}| + |G_{I_{ad}(\mathbf{r}_i|\hat{s})}|. \tag{7}$$

We show the sampling function, $S(\hat{s})$, in Figs 6 and 7 for the normal and reverse polarity site distributions. It is apparent from these figures that the sediment records sample the equatorial and low latitudes particularly well within the rather restricted longitudinal range spanned by the oceanic cores. However, despite the large number of cores in the North Pacific, the CMB at mid-latitudes in the North Pacific is comparitively poorly sampled because the inclination data

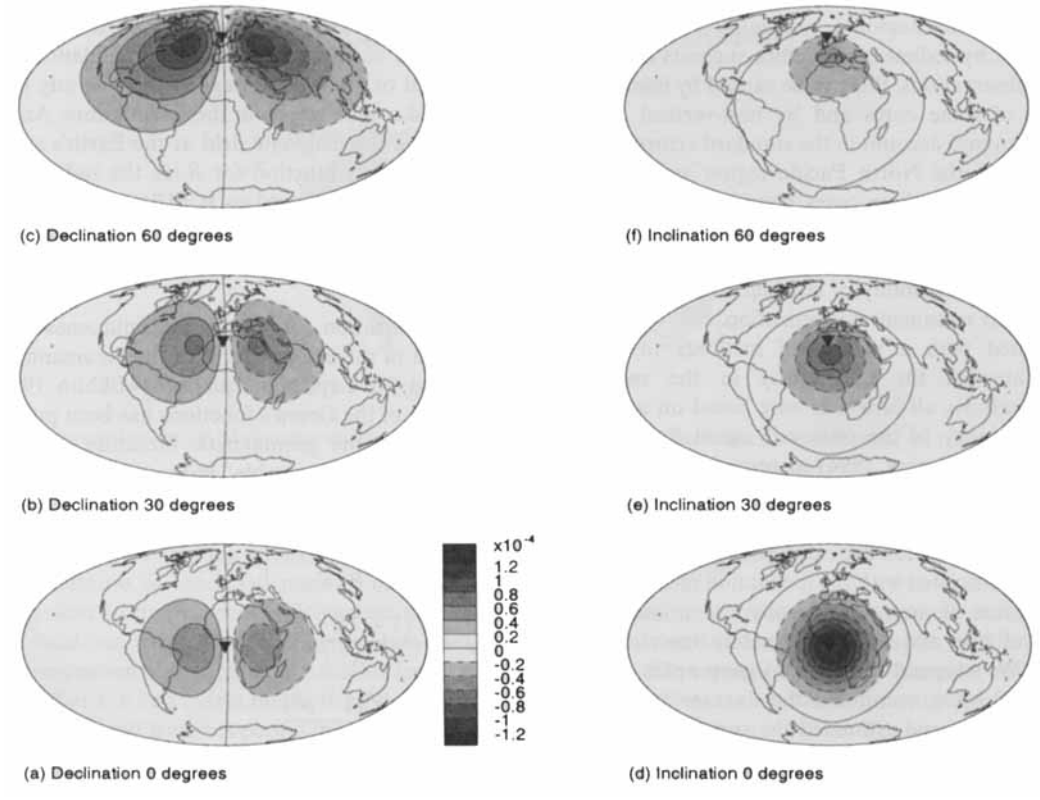

Figure 5. Linearized kernels, showing the sampling of the radial field at the CMB for an observation of declination or inclination data at (a,d) (0°N, 0°E), (b,e) (30°N, 0°E), (c,f) (60°N, 0°E). Good longitudinal and high latitude sampling requires both inclination and declination data.

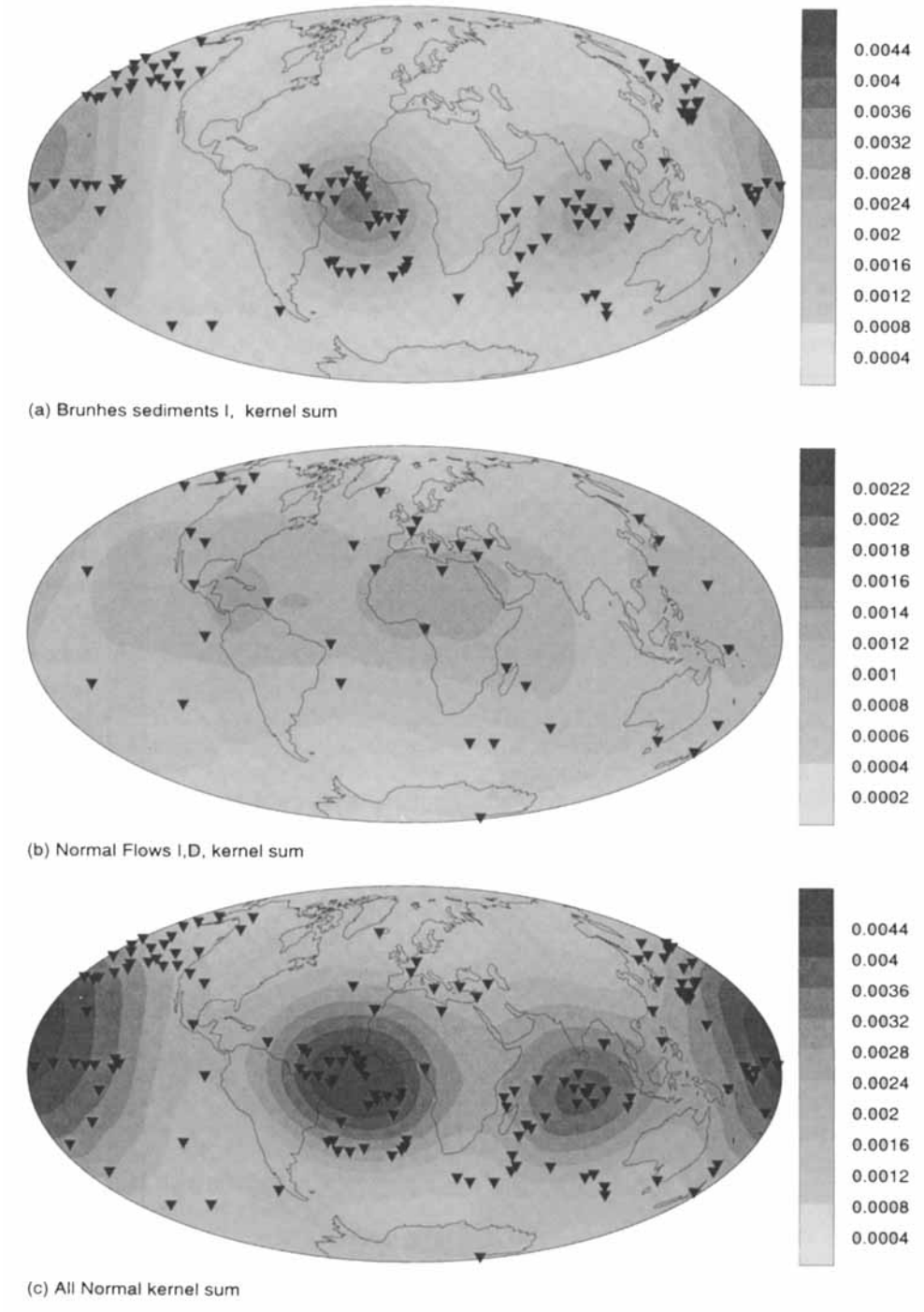

Figure 6. Sampling of the core–mantle boundary as defined by our sampling function (see text, eq. 7) for (a) Brunhes sediments, only inclination data available; (b) normal lava-flow data, both declination and inclination available (note the difference in scale due to a small number of data); (c) combined normal polarity lava-flow and sediment data sets. The combined data set shows the best spatial sampling.

kernel is biased towards latitudes lower than that of the observation site. The lava-flow data also have significant lows in the sampling function, particularly at high latitudes. However, the combined coverage is a significant improvement over that obtained from the individual data sets, in part because the continental sites for many of the lava flows provide complementary coverage to the oceanic sediments. The best sampled regions are at low to mid-latitudes beneath the ocean basins. We note here that although S indicates which parts of the CMB the observations are sampling, it does not offer any indication of the kind of resolution we can expect in our models. We discuss this in more detail later.

5 ZONAL TIME-AVERAGED FIELD MODELS

Before discussing time-averaged field models incorporating longitudinal (non-zonal) structure, we first examine whether zonal models can adequately describe the signal in both the individual lava-flow and sediment data sets, and in the

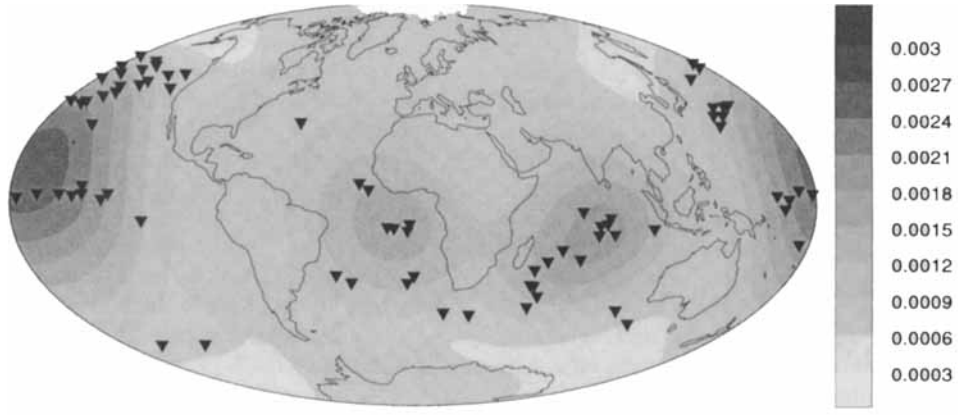

(a) Matuyama sediments I, kernel sum

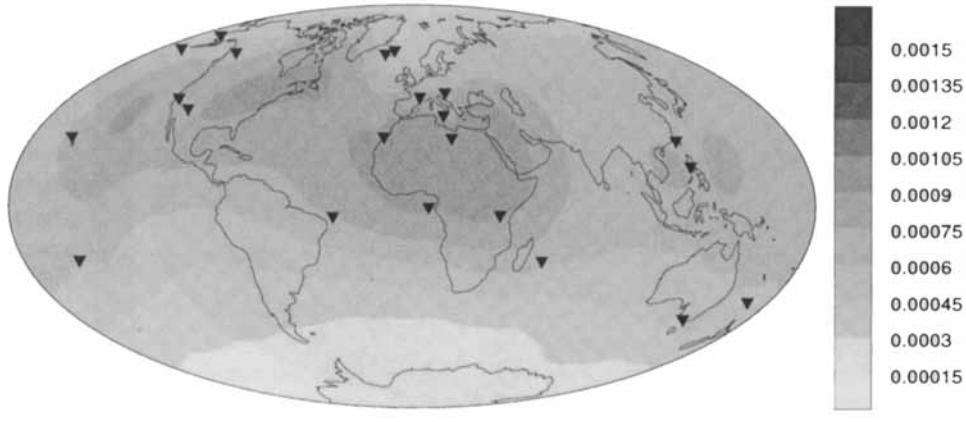

(b) Reverse Flows I,D, kernel sum

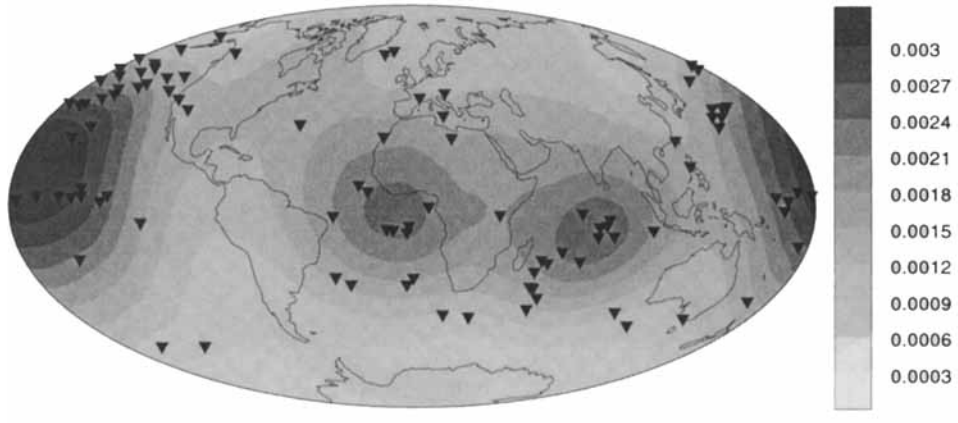

(c) All Reverse kernel sum

Figure 7. As in Fig. 6 but for (a) Matuyama sediments, only inclination data; (b) reverse lava-flow data, declination and inclination data (note difference in scale); (c) combined reverse lava-flow and sediment data sets. Notice the poorer sampling compared with that of the normal polarity data sets.

combined data set. As in JC95, we initially require that models fit our data to within the 95 per cent confidence limit on the expected value of χ^2_N. This assumes that our data uncertainties have a Gaussian distribution, with a mean and variance representative of the true mean and variance of the underlying statistical distribution from which the observations are drawn. We shall see later (Section 7) that this assumption is not valid for the combined lava and sediment data set—on average, our data uncertainties need to be increased by 10–30 per cent.

We refer the reader to JC95 (Table 2 and text) for details of zonal modelling of the lava-flow data alone, and simply reiterate the main conclusion, which is that zonal models cannot describe the signal in the lava-flow data. Note that although the lava-flow uncertainties are slightly smaller in this paper than in JC95, the conclusion that zonal models do not fit the data still holds since the smaller errors mean that it is harder to fit the data to a given RMS misfit. The zonal models include terms up to spherical harmonic degree 20 (including terms beyond about degree 10 has no influence on the resulting models: thus the effects of truncation are negligible).

In contrast to the flow data, the sediment inclination observations are fitted adequately by a zonal TAF. Table 2 shows

Table 2. Zonal models for sediment data.

Brunhes Sediment Models

Model	*Data*	*N*	*RMS*	R_1	g_2^0	g_3^0	g_4^0	*Itⁿ#*	*Weights*
B1	All	158	1.17	0.93	2.1	-2.3	-0.7	4	Uniform 4°
B2	All	158	1.20	0.12	2.2	-0.2	-0.1	1	Uniform 4°
B3	< 30°N	104	1.20	0.03	1.2	-0.1	-0.1	1	Uniform 4°
B4	All	158	1.20	0.08	1.8	-0.1	-0.1	1	3.5°, 5.0°
B5	SK90	175	5°	N/A	2.6	-2.9	N/A	N/A	least squares fit

Matuyama Sediment Models

Model	*Data*	*N*	*RMS*	R_1	g_2^0	g_3^0	g_4^0	*Itⁿ#*	*Weights*
M1	All	101	1.20	0.49	4.1	-0.6	-0.4	2	Uniform 4°
M2	< 30°N	62	1.20	0.33	3.7	-0.2	-0.2	1	Uniform 4°
M3	All	101	1.20	0.48	4.1	-0.4	-0.4	2	3.5°, 5.0°
M4	SK90	125	6°	N/A	4.6	-2.1	N/A	N/A	least squares fit

N is number of data in the inversion; RMS is RMS misfit of model to data. (In the case of models B5 and M4, the RMS is in degrees, since the data were not weighted in the least-squares fit.) R_1 is model roughness parameter, based on smoothness constraint which minimizes the RMS radial field at CMB. g_2^0, g_3^0 and g_4^0 are the first three zonal spherical harmonic coefficients in the models. In models B4 and M3, data uncertainties of 3.5° were used for cores between latitudes 30°S and 10°N, and uncertainties of 5° were used for cores from higher latitudes.

the results of regularized inversions of the Brunhes and Matuyama sediment data for smooth zonal models, using a variety of data weighting schemes. In every case the RMS misfit lies within the 95 per cent confidence limit for the expected value of χ^2. The data in these inversions are not binned spatially, as the aim of the exercise was to see whether zonal models are sufficient to describe even the unsmoothed data. The models are compared with previous least-squares fits to the data (SK90). It can be seen that average data uncertainties on the order of 4° are consistent with zonal models for the sediments, although the magnitudes of individual spherical harmonic coefficients are rather poorly constrained and are significantly affected by the distribution of the uncertainties. In all cases, though, the main contribution to the models comes from the axial quadrupole term, and this term is larger for the Matuyama data than for the Brunhes data (see also Schneider & Kent 1988, 1990). Inversions of the binned sediment data sets yield the same general conclusions.

Table 3 shows the RMS misfits of zonal models to the combined sediment and flow data sets. Again, the zonal models include terms up to spherical harmonic degree 20. The required RMS (third row of Table 3) is the 95 per cent confidence limit on the expected value of χ^2_N, and it is clear that zonal models cannot fit the data to within this tolerance limit. In the next section we shall see that more realistic estimates of the required RMS misfit to the data are given by the values in the last row in Table 3. Even with this increase in average misfit, zonal models are inadequate to describe the combined data sets.

6 NON-ZONAL FIELD MODELS—AN EXAMPLE

In this section we present a detailed example of a full non-zonal inversion of the 0–5 Ma normal polarity combined sediment and lava-flow data, to illustrate some of the issues which must be considered in obtaining reliable models of the time-averaged field structure. Existing models for the time-averaged field show large variations in the amount of structure they contain: this is in part due to differing data sets and techniques, but also to *a priori* biases about how well we can fit the palaeomagnetic data. We show here that careful consideration of the details of each inversion of the data is

Table 3. Zonal models for combined sediments and lava flows.

	Brunhes (N = 146)		*Normal (N = 149)*		*Reverse (N = 96)*	
	RMS (R_1)	*RMS* (R_2)	*RMS* (R_1)	*RMS* (R_2)	*RMS* (R_1)	*RMS* (R_2)
RMS – GAD model	1.53	1.53	1.78	1.78	2.10	2.10
RMS – zonal model	1.34	1.35	1.50	1.52	1.75	1.77
Required RMS 1	1.15	1.15	1.15	1.15	1.18	1.18
Required RMS 2	1.25	1.25	1.40	1.40	1.50	1.50

Required RMS 1 = RMS misfit required using a tolerance level given by the 95 per cent confidence interval on the expected value of χ^2. Required RMS 2 = RMS misfit required in the full non-zonal inversions discussed in Section 8. Criteria for choosing this RMS are given in Section 7. RMS(R_1) and RMS(R_2) indicate RMS misfits to zonal models using minimum RMS radial field and RMS surface gradient norms, respectively.

necessary. In particular, we demonstrate that the uncertainty estimates derived for the data in Section 4 are almost certainly too optimistic: using these we are often unable to guarantee finding the minimum norm model as desired in Occam's process. The analyses presented below result in the important conclusion that, after consideration of the trade-off between roughness and misfit, the uncertainties in the data need to be increased by 10–30 per cent.

The inversion procedure used here is an iterative non-linear algorithm (Constable *et al.* 1987; Parker 1994; Johnson & Constable 1995) where at each iteration (i) a new model is computed from a linearization about the model from the previous iteration ($i-1$). The new model is given by

$$\mathbf{m}_i = [\lambda R^{\mathrm{T}}R + (WJ_{i-1})^{\mathrm{T}}(WJ_{i-1})]^{-1}(WJ_{i-1})^{\mathrm{T}}W\hat{\mathbf{d}}_{i-1}, \qquad (8)$$

where $\mathbf{m}_i$ is the new model, J_{i-1} is the Jacobian evaluated at the model from the previous iteration ($\mathbf{m}_{i-1}$), W is the matrix of data uncertainties diag$\{1/\sigma_1, 1/\sigma_2, \ldots, 1/\sigma_N\}$, R is the smoothness or regularization constraint, λ is the Lagrange multiplier and d_{i-1} is a linearization of the data about the model $\mathbf{m}_{i-1}$. Thus λ represents the trade-off between fitting the data and obtaining a smooth model. A large value of λ means that smooth models will be obtained; in contrast a value of zero for λ results in a least-squares solution for $\mathbf{m}_i$. At each iteration in the inversion, a range of values of λ are used, and the corresponding model, $\mathbf{m}_i$, and RMS misfit of $\mathbf{m}_i$ to the data computed. The preferred new model saved from each iteration is the one corresponding to the minimum in the RMS misfit versus λ curve for that iteration. In a well-behaved inversion, the minimum in the RMS misfit versus λ curve at each iteration corresponds to a misfit lower than the misfit of the model from the preceding iteration. We refer to iterations early in the inversion, where the minimum RMS misfit is greater than the required tolerance level, as phase 1 of the inversion (see Parker 1994, chapter 5, section 5.04).

Fig. 8 shows the behaviour of λ, the RMS misfit and the model roughness as a function of iteration number for an inversion of the full 0–5 Ma normal polarity data set (sediments and flows). Also shown is the trade-off curve of model roughness versus misfit. Non-zonal structure is allowed in the inversion and the smoothness constraint is a minimization of the RMS value of the radial magnetic field at the CMB. The starting model is a GAD, as in all our inversions, and the maximum spherical harmonic degree and order are 10. Fig. 9 shows the radial field models (plotted at the CMB in μT) for selected iterations from the inversion. Initially the inversion is well-behaved with a decrease in RMS misfit, accompanied by a gradual increase in the model roughness (Figs 8 and 9). From iteration 14 onward, there is a marked change in the character of the inversion—at iteration 15 the models suddenly become much rougher and the inversion proceeds in a much less stable manner, with sudden decreases in misfit accompanied by corresponding increases in model roughness. The trade-off curve is no longer smooth and indeed we can see from Figs 8 and 9 that it is possible to obtain models which have a lower misfit, but are smoother than models from a previous iteration (e.g. the model at iteration 17 versus the model at iteration 15). This kind of behaviour is the result of a numerical stability procedure which is incorporated into the Occam algorithm (Constable *et al.* 1987). The procedure comes into play if the minimum in the RMS misfit versus λ curve for iteration i is larger than the misfit of model, $\mathbf{m}_{i-1}$, from

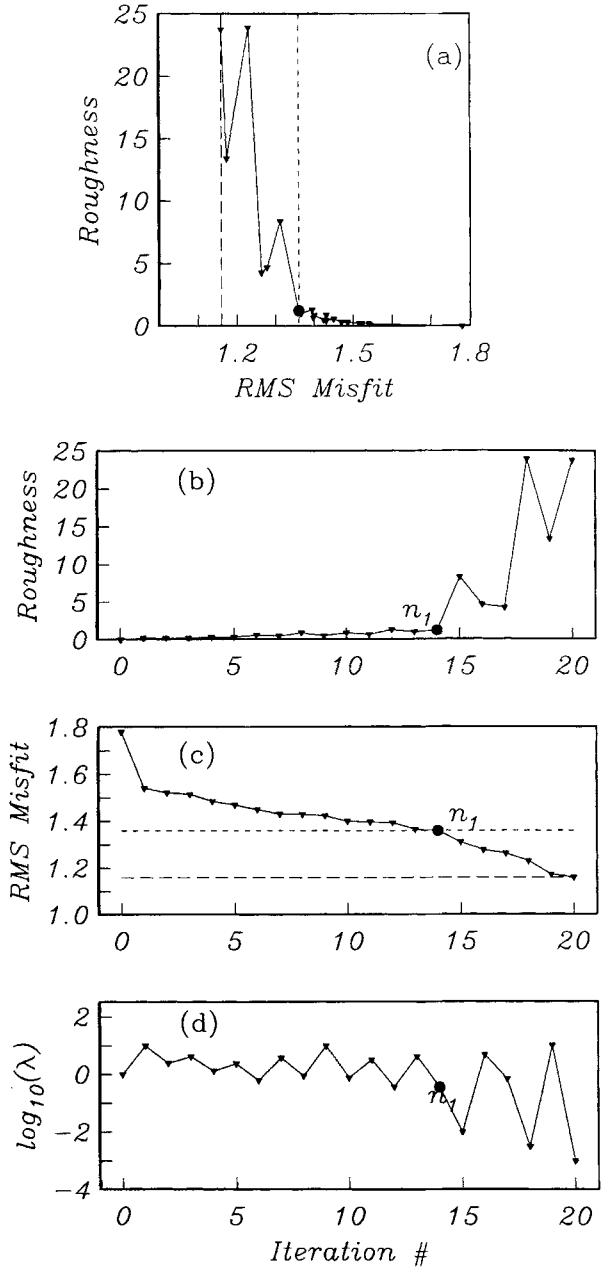

Figure 8. Regularized inversion of normal polarity lava-flow and sediment data. (a) Trade-off curve. The vertical dashed line is the required RMS misfit based on 95 per cent confidence limit on $E(\chi^2)$. The vertical dotted line is the desired RMS misfit based on characteristics of inversion (see text). (b), (c) and (d) show model roughness, RMS misfit and Lagrange multiplier, λ, respectively, versus iteration number during the inversion. Misfit levels in (c) are as in (a). n_1 denotes iteration defining the division between two different behaviour regimes in the inversion (see text).

the previous iteration, and also larger than the required tolerance level to fit the data. In other words, phase 1 of the inversion is not well-behaved [see Parker 1994, chapter 5.04; the examples in Parker (1994) are 'well-behaved' linearizations, unlike the example given in Figs 8 and 9 here]. In the stabilization procedure, the new model at the ith iteration is computed using

$$\mathbf{m}_{\mathrm{new}} = f\mathbf{m}_i + (1-f)\mathbf{m}_{i-1}, \qquad (9)$$

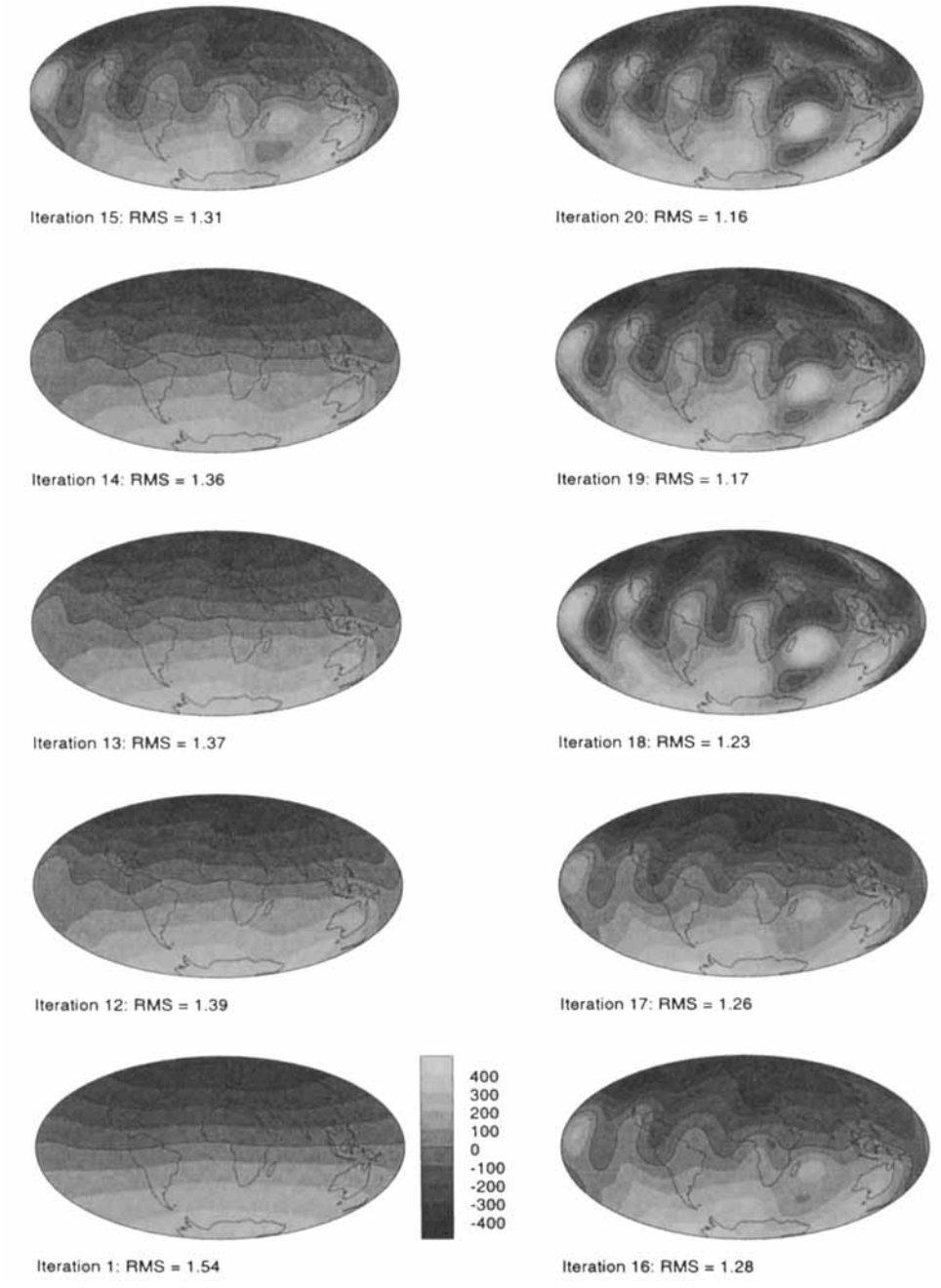

Figure 9. Field models for selected iterations from the inversion shown in Fig. (8). Model is plotted in terms of the radial field, B_r, at the CMB. Units are μT; contour interval is 100 μT. RMS misfit at each iteration is given. Note the marked change in character of inversion between iterations 14 and 15.

where $0 < f < 1$, $\mathbf{m}_i$ is given by eq. (8), and $\mathbf{m}_{i-1}$ is the model solution from the previous iteration. RMS misfit versus λ is computed for successively decreasing value of f, until the minimum in the RMS–λ curve is less than the RMS misfit of model $\mathbf{m}_{i-1}$. Although numerical stability is retained, the model resulting from eq. (9) is no longer a minimum norm model in the sense of a true regularized inversion.

Fig. 10 shows the trade-off curve from an inversion of the same normal polarity data set, but using a stronger smoothness constraint (minimum dissipation norm, *cf.* Gubbins & Bloxham 1985; Gubbins & Kelly 1993; Kelly & Gubbins 1997). Similar behaviour occurs during the inversion, although the misfit level at which the linearization breaks down (iteration n_1, Fig. 10) is slightly higher than in Fig. 8, reflecting the heavier damping imposed by the diffusion norm. It can be seen that if the inversion proceeds to a small enough RMS misfit (iteration n_2, Fig. 10), the trade-off curve becomes smooth again; however, a further decrease in misfit can only be obtained at the expense of very rough models, and the inversion is constrained by the search range of the Lagrange multiplier.

The above discussion shows that if the required RMS misfit of the data to our model lies beyond the critical iteration, n_1, at which the onset of linearization problems begin, many complications can occur. Beyond n_1, any models obtained will

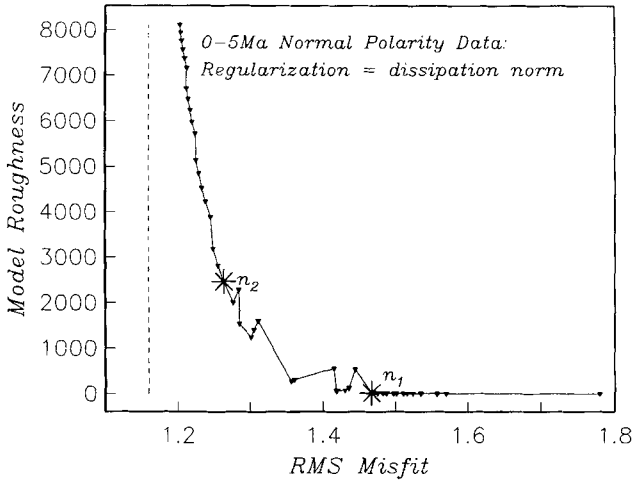

Figure 10. Trade-off curve for inversion of normal polarity lava-flow and sediment data, as in Fig. 8(a), but using a stronger regularization constraint (minimization of ohmic dissipation norm). The vertical dashed line is the required RMS misfit based on the 95 per cent confidence limit on $E(\chi^2)$. Inversion shows similar characteristics to that shown in Fig. (8).

not be maximally smooth solutions to the inversion. Small changes in the input data set (e.g. deleting one site during a jackknife inversion) can lead to vastly different final models with the same RMS misfit of the data. Thus jackknife estimates of the variance in the model will be huge, reflecting the intrinsic instability of the inversion, which in turn results from the fact that at some level the data are inconsistent and the problem is no longer linearizable. Similarly, consider two models A and B with the same RMS misfit, but where model B was computed using a heavier smoothness penalty than model A. If the RMS misfit of the models corresponds to an iteration higher than the critical iteration, n_1, then model B may actually be rougher than model A, even though a heavier damping was imposed! Obviously this kind of behaviour is undesirable in any modelling algorithm—we detail it purely to point out some of the otherwise somewhat obscure pitfalls of overfitting the palaeomagnetic data. Note that problems of this kind have not previously been encountered with the Occam algorithm, despite the wide range of non-linear geophysical inversion problems on which it has been tested.

Behaviour similar to that outlined above was observed for the Brunhes, normal and reverse data sets modelled here, and were found regardless of whether declination data were included in the inversion. Thus, in contrast to JC95, we did not use the 95 per cent confidence limit on the expected value of χ^2 as the required misfit of our final models to the data. Instead we selected an RMS misfit for each of the data sets, so that the rough part of the trade-off curve described above and seen in Figs 8–10 was never reached. The revised required RMS misfits for each of the subsets of data modelled are given in Table 3. For each subset of the data, this revised RMS was selected by running the inversion until the data were fitted to an RMS given by the 95 per cent confidence limit on the expected value of χ^2, carefully examining the characteristics of the inversion (for example, see Figs 8 and 9) and choosing the new RMS misfit level by identifying the iteration in the inversion corresponding to n_1 in Figs 8 and 9. The revised misfits do not alter the conclusion that zonal models do not fit the data. Fitting the data to these RMS misfits is equivalent to a variance reduction of 33, 38 and 49 per cent for the Brunhes, 0–5 Ma normal and 0–5 Ma reverse data subsets, respectively. The greater variance reduction achieved for the reverse polarity data subset is a consequence of higher signal-to-noise ratio in the data. The sparser reverse data distribution may also contribute to the variance reduction by allowing more efficient regularization of the model. One difference between the Occam's inversion technique used here and the approach used by Kelly & Gubbins (1997) is that, rather than seeking the value of λ corresponding to minimum structure in the resulting model, they fix the value of λ prior to inversion. Differences between these two approaches are illustrated by Parker (1994, Figs 5.04a and 5.05e). For similar RMS misfit to the data and the same kind of model norm, we expect that the two procedures should produce very nearly the same models. This seems to occur, although given the non-linearity of the problem there are no guarantees that the different routes followed in constructing a solution will arrive at the same models, or indeed that either of these will be at the global minimum for the penalty functional.

7 RESULTS—NON-ZONAL TIME-AVERAGED FIELD MODELS

Non-zonal models out to degree and order 10 were obtained for the Brunhes, 0–5 Ma normal and 0–5 Ma reverse data sets. The required RMS misfit for the final models for each subset of data is given in Table 3. Because of the regularization constraint and the non-uniform data distribution, the 119 spherical harmonic coefficients in the inversion are not uncorrelated. Beyond spherical harmonic degree 4, the actual values of the spherical harmonic coefficients are strongly constrained by the regularization used in the model; however, by using a maximum spherical harmonic degree of 10, we ensure (as in JC95; Kelly & Gubbins 1997) that the final models are not influenced by the cut-off in the spherical harmonic expansion.

From our earlier inversions (JC95) using only lava-flow data, we concluded that differences between our Brunhes and 0–5 Ma normal models were probably the result of different data distributions and possibly inadequate temporal sampling at a few sites. Incorporation of sediment data into the inversions has confirmed this conclusion as we find that models specified in terms of B_r at the CMB obtained from inversions of just the Brunhes data, and with an RMS misfit given by the last row in Table 3, are almost identical to models for all of the normal polarity data. Further results and discussions in this paper therefore pertain solely to the 0–5 Ma normal and reverse data subsets. Figs 11(a) and (b) show the field models for normal and reverse polarity data. The model is plotted in terms of the radial field at the CMB, for comparison with historical field maps and other recent palaeofield maps (JC95; Gubbins & Kelly 1993; Kelly & Gubbins 1997). We refer to these models as LSN1 (normal) and LSR1 (reverse). Spherical harmonic coefficients for models LSN1 and LSR1 out to degree and order 4 are given in Table 4. Declination and inclination residuals to these models are shown in Fig. 12. The residual is defined as the observed average field direction (inclination or declination) minus the model prediction, normalized by the data uncertainty. Because we are now fitting the data to an RMS misfit greater than that given by the 95 per cent confidence interval on the expected value of χ^2 (i.e.

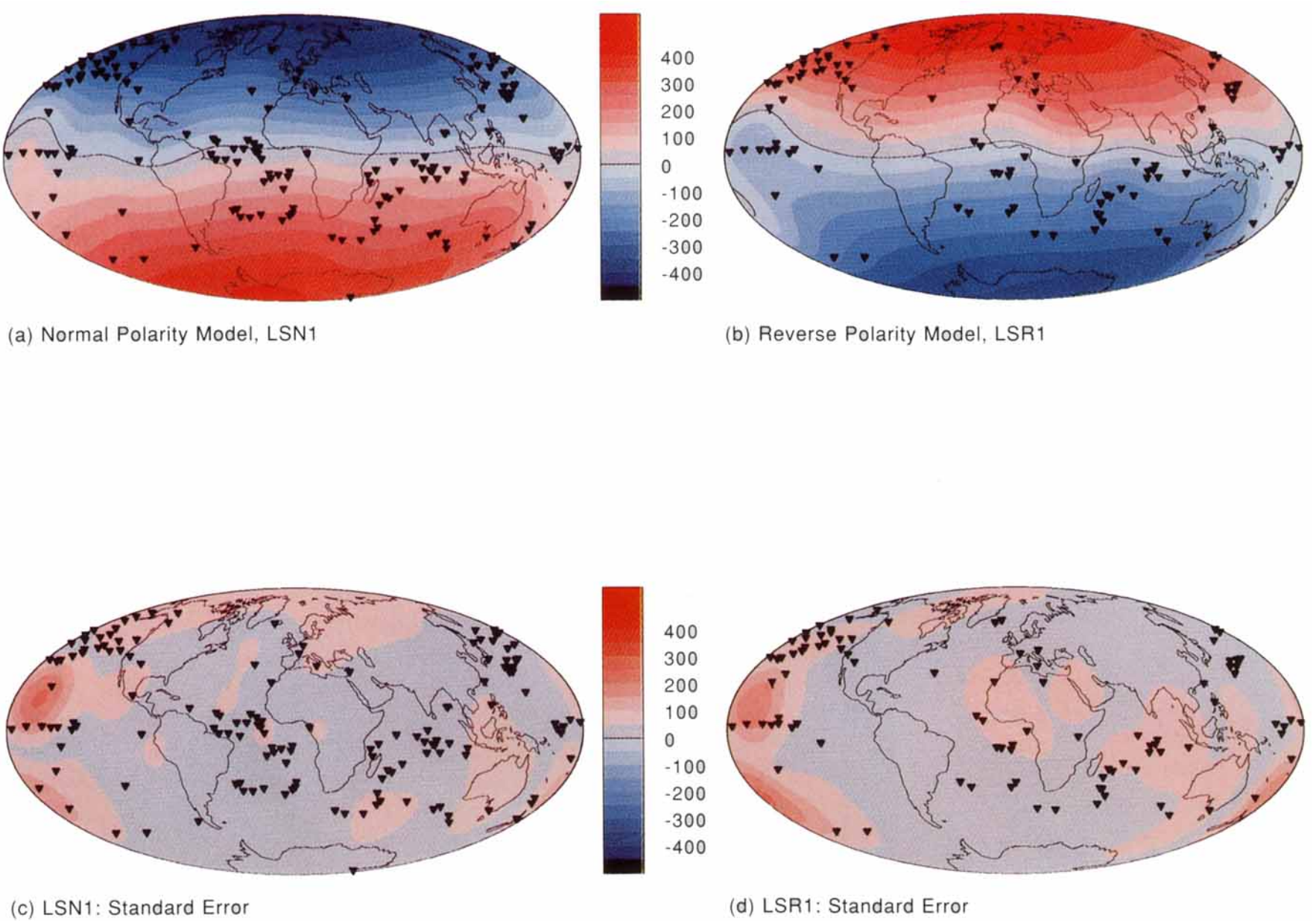

Figure 11. (a) normal (LSN1) and (b) reverse (LSR1) field models from combined lava-flow and sediment data, shown in terms of B_r, at the CMB. Units are μT; contour interval is 50 μT. Also shown are jackknife estimates of standard error in B_r for (c) LSN1 and (d) LSR1. Normal and reverse data locations are indicated as appropriate (triangles).

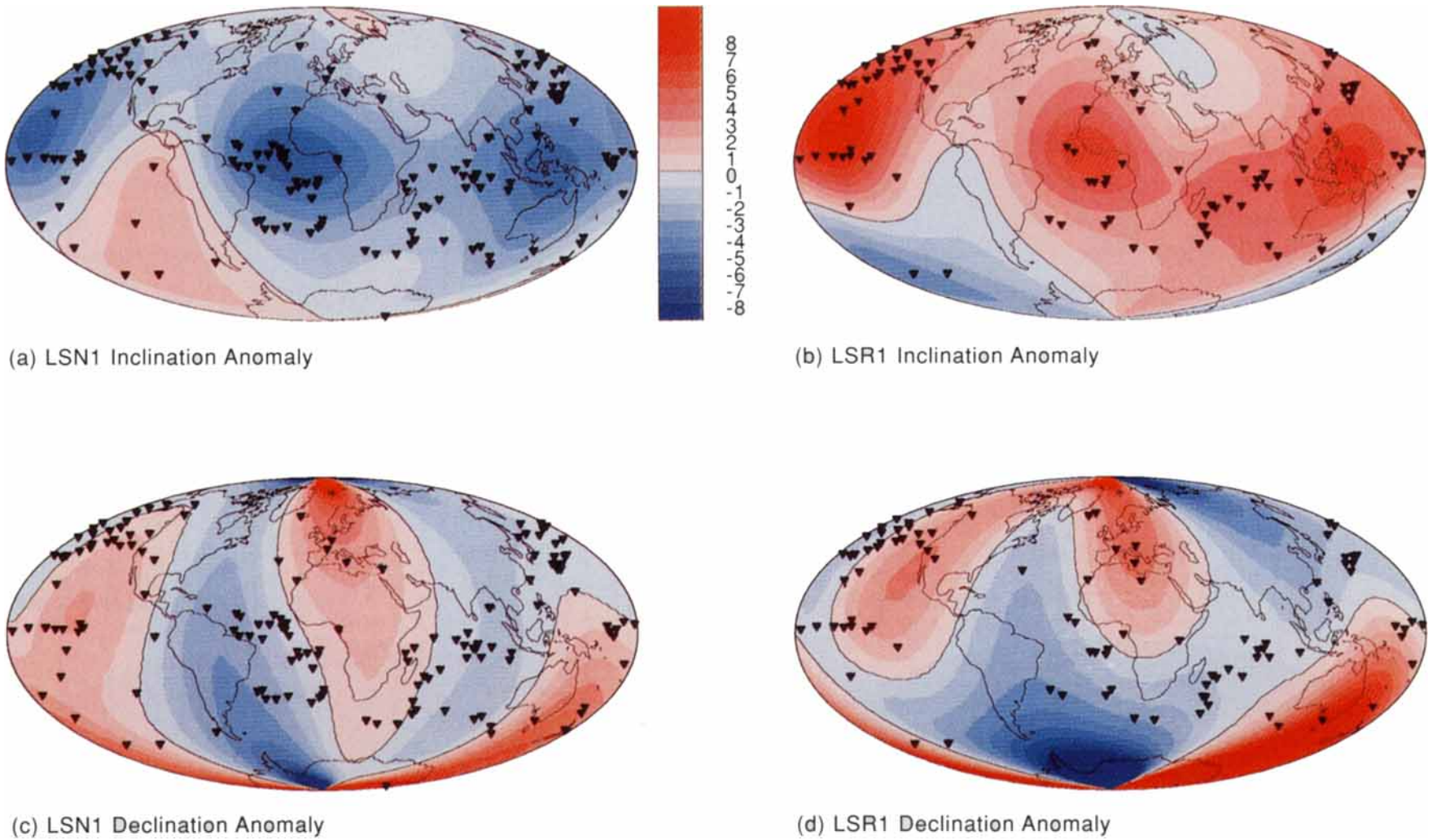

Figure 13. Inclination (a, b) and declination anomilies (c, d) relative to a GAD field predicted by models LSN1 and LSR1. Anomolies are plotted at the Earth's surface. The contour interval is 1°. Data locations are shown (triangles)

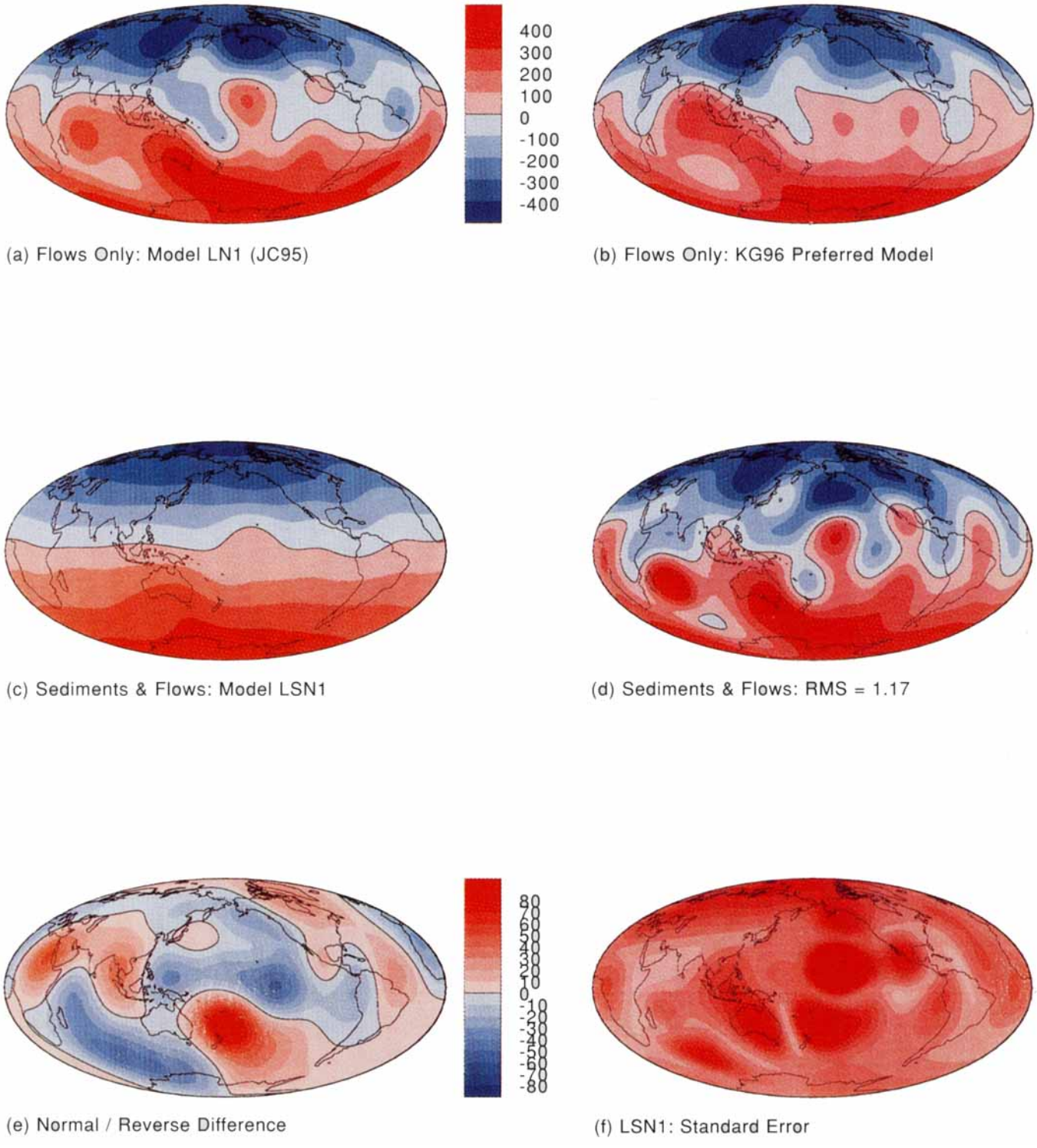

Figure 15. Comparison of time-averaged field models, all plotted in the Pacific Hemisphere. (a) LN1 of *Johnson & Constable* (1995)–lava flows only; (b) *Kelly & Gubbins* (1997)–lava flows only; (c) LSN1–lava flows and sediments, this paper; (d) normal polarity model for lava flows and sediments with RMS = 1.17, this paper. (e) shows the sum of LSN1 and LSR1 to highlight asymmetries between normal and reverse polarity field models. (f) is the uncertainty in LSN1, as in fig. 11(c), but plotted in the Pacific Hemisphere for consistency. Note the difference in scale for the lower two figures.

Table 4. Spherical harmonic coefficients for models LSN1 and LSR1.

		Normal PolarityModel, LSN1		Reverse PolarityModel, LSR1	
l	m	g_l^m	h_l^m	g_l^m	h_l^m
1	0	-30.000000	0.000000	30.000000	0.000000
1	1	0.116804	0.312925	-0.096547	-0.503837
2	0	-1.084134	0.000000	1.153622	0.000000
2	1	-0.162684	-0.494206	0.681404	0.926910
2	2	0.324327	-0.280945	-0.172222	0.156342
3	0	-0.284591	0.000000	0.350477	0.000000
3	1	0.060307	-0.108124	-0.164206	-0.136731
3	2	0.085893	0.089452	-0.414254	-0.089291
3	3	0.136414	-0.138830	-0.232005	0.148598
4	0	0.044126	0.000000	-0.072430	0.000000
4	1	0.082816	0.087568	-0.134981	-0.092969
4	2	-0.009701	-0.094280	0.049117	0.119187
4	3	-0.058086	-0.080475	0.050938	0.114522
4	4	-0.036387	0.018488	0.079818	0.011461

l = spherical harmonic degree; m = order; g_l^m, h_l^m = spherical harmonic coefficients in μT

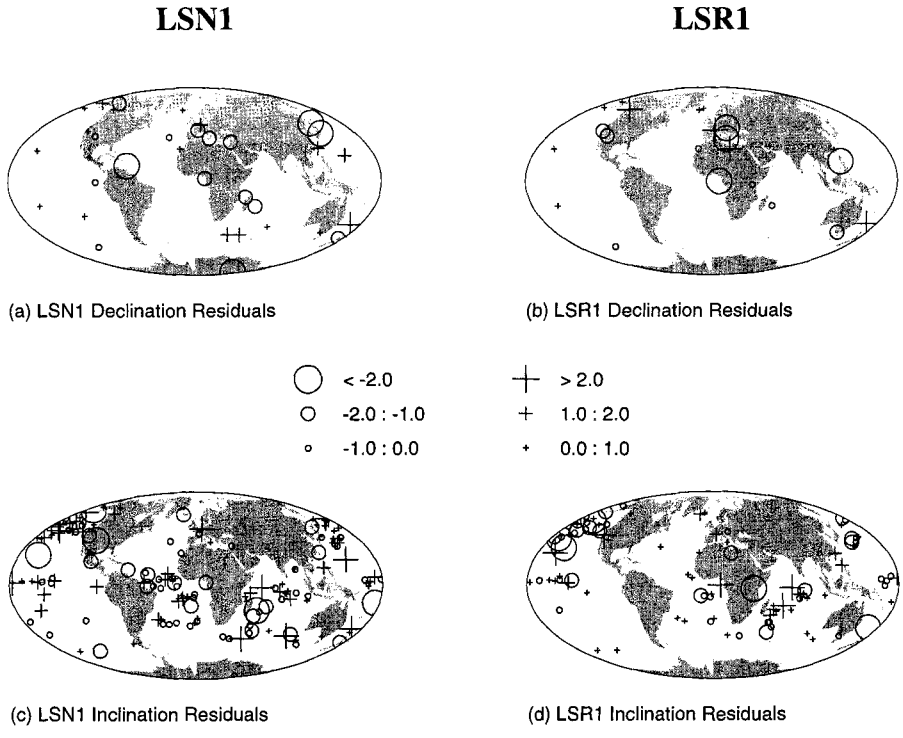

Figure 12. Declination (a, b) and inclination (c, d) residuals to models LSN1 and LSR1. Negative residuals are denoted by circles, positive residuals by plus signs; the size of the sign corresponds to the magnitude of the residual as indicated by the legend.

we are fitting the data less well), the number of residuals with a magnitude greater than 2.0 has increased to approximately 12 per cent of the total number of data in the inversion. The large residuals generally occur in regions where the data coverage is good, but where the inclination and/or declination anomalies themselves are inconsistent in sign or magnitude.

The primary non-zonal structure in both LSN1 and LSR1 is the anomalous radial field in the Pacific. LSN1 and LSR1 appear to have similar non-axial-dipole structure, but the reverse field shows a slightly greater deviation from a GAD than the normal field, consistent with the larger-magnitude inclination anomalies observed in the reverse data (Figs 2–4).

The model norm for the 0–5 Ma normal polarity data is substantially lower than for reverse polarity: the RMS value of the non-axial-dipole contribution to B_r on the CMB is 27.8 μT for normal 0–5 Ma and 39.6 μT for reverse 0–5 Ma. Note that LSN1 and LSR1 are smoother than their lava-flow-only counterparts, LN1 and LR1 (JC95), and the differences between the normal and reverse field have been reduced considerably. This results in part from the addition of a large amount of sediment data, which on their own do not require non-zonal field structure; also, the RMS misfit of the models presented here is slightly larger than for LN1 and LR1. If the combined sediment and flow data sets are fitted to a misfit

level comparable to LN1, then the structure in the resulting models is greatly increased (see Fig. 9, iteration 19 or Fig. 15d). Model LSN1 is very similar in structure to model LB1 (lava flows only, Brunhes, JC95) and LN2 (0–5 Ma normal lava only with five sites removed, JC95). These observations suggest that the larger amount of structure in the previous 0–5 Ma normal polarity model, LN1, can in part be attributed to the use of additional sites with poor temporal sampling. (Remember that we have removed six lower-quality lava flow sites in model LNS1 compared with model LN1—see Table 1 and Section 4.1). LSR1 differs from both our previous reverse polarity field models in the South Atlantic because we have removed a low-quality data point from Fernando de Noronha (Table 1). Otherwise, our new reverse polarity field model is very similar to models based on the lava-flow data alone. The addition of sediment data has improved the spatial coverage in our models, but does not contribute much structure because only inclination data were available and they have larger uncertainties associated with them. The high-latitude flux lobes observed in historical field models and in our previous normal polarity field model, LN1, are not observed in models LSN1 and LSR1. However, models for the combined sediment and lava-flow data sets with a lower RMS misfit than LSN1 and LSR1 do show high-latitude flux lobes, although the positions and morphology of the lobes are poorly constrained. Thus the absence of flux lobes in our new models does not necessarily imply that such features do not persist over the last 5 Myr, but rather that we cannot detect them given the quality and distribution of current data sets.

Uncertainties in our models are estimated using the jackknife technique (see e.g. Miller 1974; Efron 1982). One site at a time is deleted from the data set and an inversion of the remaining $N-1$ sites performed. N 'delete-1' estimates of the model $(\hat{s}_j, j = 1, 2, \ldots, N)$ are obtained and the standard error is given by $v = \sqrt{\mathrm{Var}(B_r)}$, where

$$\mathrm{Var}(B_r) = \frac{N-1}{N}\left\{\sum_{j=1}^{N}(\hat{s}_j^2) - \frac{\left(\sum_{j=1}^{N}\hat{s}_j\right)^2}{N}\right\}. \quad (10)$$

In our previous study we quoted just the error estimates in the spherical harmonic coefficients (Table 3, JC95); this is somewhat misleading as the regularization and site distribution impose a covariance on the spherical harmonic coefficients which is not described by the jackknife standard error estimates. Here we show instead the jackknife estimate of the standard error in the radial field at the CMB for each of our models (Figs 11c and d), as we are more interested in the structure of our field models than in the absolute values of the spherical harmonic coefficients. An important caveat regarding these jackknife error estimates is that small standard errors can be generated for two reasons, only one of which may have anything to do with accuracy of the models. If data are regionally consistent there will be little effect if one data point is deleted, and the model will appear reliable in the region sampled by those data. However, if there is poor sampling of some region on the CMB, the dominant influence on the models will be the regularization of the inversion, tending to minimize the non-axial-dipole contribution to the field. The regularization influence will dominate the model structure in that region, regardless of which data are deleted. Thus small values of the standard error in Figs 11(c) and (d) should not necessarily be taken to indicate that the model is well determined in that region. Comparison of the standard error figures with the sampling functions in Figs 6(c) and 7(c) shows that low standard errors from the jackknife procedure are often associated with poorly sampled areas.

The most obvious feature in the jackknife error maps is the large standard error associated with the main non-zonal feature in the models—the Pacific anomaly. Analysis of all the 'delete-1' estimates of models LNS1 and LSR1 show that the magnitude of the Pacific anomaly is controlled by lava-flow data from Hawaii, but its existence is consistent with data from equatorial Pacific sediment cores. The amplitude of the anomaly required by the cores is smaller than that required by the Hawaiian lava-flow data, because the sediments have smaller inclination anomalies and larger uncertainties. Previous studies have suggested that serial correlation and inadequate temporal sampling contribute to anomalous average field directions at Hawaii; we do not believe that to be a serious problem here since data are available from several volcanic sequences from different islands in the chain, and therefore are of different ages. However in light of a recent study of the effects of serial correlation on estimates of secular variation at Hawaii (McElhinny, McFadden & Merrill 1996b), we address the issue of the Hawaiian record in some detail in a separate section below.

Declination and inclination anomalies predicted by models LSN1 and LSR1 are shown in Fig. 13. The improved spatial data distribution in these models compared with those based on lava-flow data alone results in much smoother inclination and declination anomaly maps. As with the field models in Fig. 11, it can be seen that the non-zonal structure in the normal and reverse polarity models is very similar. Maximum inclination anomalies occur in the South Atlantic, central Pacific and Indonesia, near the best spatial data coverage. Positive declination anomalies are seen over Europe, extending down through Africa and over western North America and the East Pacific. The magnitudes of the declination anomalies for the normal polarity field models are almost everywhere less than 3°. In areas where we have good data coverage, both the declination and the inclination anomalies are, on average, slightly larger for LSR1 than for LSN1 (consistent with the raw data), although the difference is much reduced compared with the models based on lava-flow data alone (JC95, Fig. 12).

In light of the ambiguity associated with the jackknife uncertainty estimates, it is worth considering what effect our choice of regularization has on the models derived here. Fig. 14 shows a suite of models for both normal and reverse polarity constructed using three different norms: the penalty on high spherical harmonic degree structure will be increasingly severe for the minimum RMS radial magnetic field at the CMB, the minimum RMS surface field gradient at the CMB, and the minimum ohmic dissipation norm. The misfit in each case is almost the same, and we see that the heavier smoothing constraints do result in models with less structure. However, a contributing effect is also that, with the heavier smoothing constraint, it is not possible to fit the data as well without encountering the problems associated with linearization described in Section 7 (compare Figs 8a and 10). We choose the radial field norm, because it gives the best regional resolution, but it is clear from Fig. 14 that the general results are very similar for other forms of regularization too.

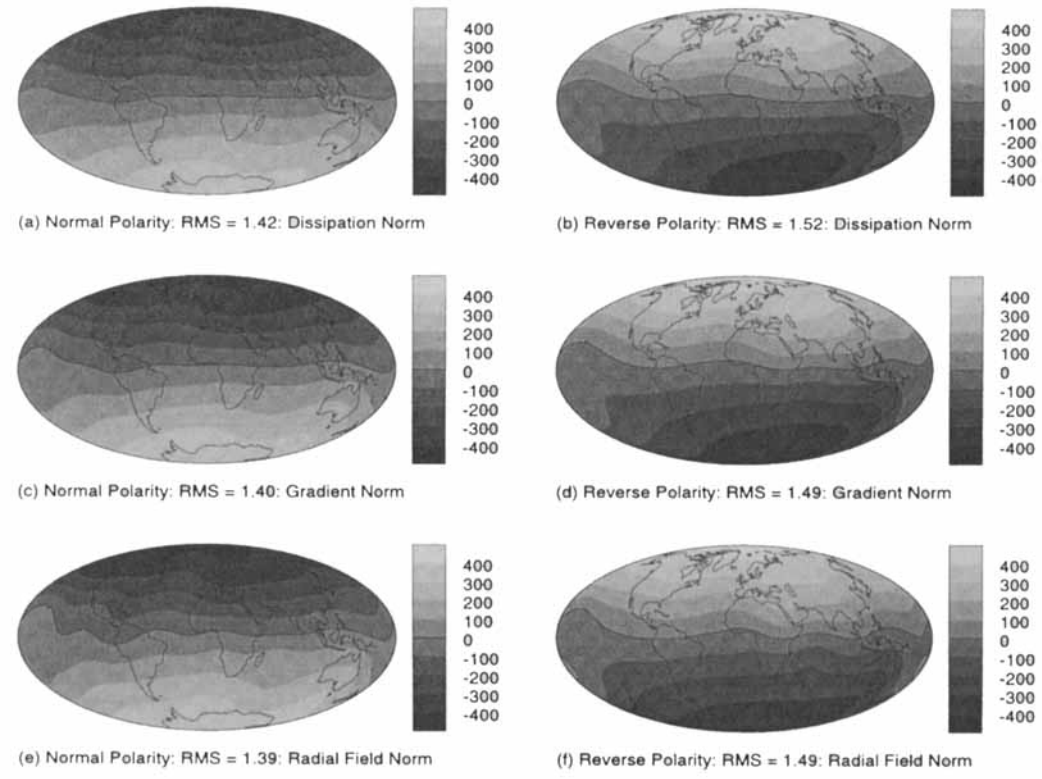

Figure 14. Field models for normal (left column) and reverse (right) polarity data sets for three different regularization constraints. B_r at the CMB—contour interval is 100 μT. Misfit levels for different regularizations are similar. Smoothness constraints are: (a, b) minimum ohmic dissipation; (c, d) minimum RMS surface gradient at CMB; (e, f) minimum RMS radial field at CMB.

A potential concern is that the non-zonal structure in our models is required only by the (inherently more noisy) declination data from the flows, and might reflect local tectonic effects (block rotations) rather than real field behaviour. We verified that this is not the case: inversions using only inclination data produced almost identical field models to LSN1 and LSR1. Accounting for the effect of plate motions on our data locations demonstrated that the correlations are insignificant and did not affect the resulting field models.

8 PALAEOSECULAR VARIATION AND THE TIME-AVERAGED FIELD AT HAWAII

Several studies in the past have inferred low secular variation in the Pacific during the Brunhes epoch (the so-called 'Pacific dipole window') based on inferences of low virtual geomagnetic pole (VGP) dispersion calculated from Hawaiian lavas. McElhinny *et al.* (1996b) claim that this interpretation of the data is flawed because many of the Hawaiian flows used in such calculations are serially correlated and thus do not provide independent measurements of field directions. They developed a statistical method for thinning such data sets and demonstrated an increase (less than 0.8°) in VGP dispersion after application of their method (Table 5, this paper; Tables 1 and 2 of McElhinny *et al.* 1996b). It is also suggested that such serial correlation of flows and inferred inadequate temporal sampling of the field can lead to biased field directions, a potentially serious problem when incorporating Hawaiian data into geomagnetic field models such as those presented in this paper.

We address these issues by looking in detail at the dispersion and mean field directions recorded by the Hawaiian data contributing to our field models and discuss our results in the context of the McElhinny *et al.* (1996b) study. Table 5 gives the field directions and VGP dispersion for the volcanic sequences contributing to our normal polarity estimate of the mean field direction at Hawaii. VGP dispersion is computed either with respect to the mean pole position for each set of flows or with respect to the geographic pole and is denoted by S_V^2 and S_P^2 respectively. If Δ_i is the angular departure of the ith VGP from the mean (or geographic) pole then the angular dispersion is given by

$$S^2_{V(P)} = \frac{1}{N-1}\sum_{i=1}^{N}\Delta_i^2. \qquad (11)$$

(We do not consider the second-order effects of within-site corrections to S_V, S_P, which are about 0.15° for the Hawaiian data.) Volcanic sequences noted by an asterisk were also analysed by McElhinny *et al.* (1996b); in addition they included a more complete set of radiocarbon-dated flows and data from the Hamakua and Kau sequences. These data were not included in our original data set, as, based on documentation in the original references, we did not regard them as spanning a sufficiently long time interval to permit a good estimate of secular variation and the time-averaged field. Our data set does include palaeomagnetic data from three additional sequences, all older than 0.8 Ma. Besides extending the Hawaiian record back to 5 Myr, the Kauai, Nihoa and Oahu (Waianae) sequences may also span longer time intervals than some of the Brunhes records [Table 5; see Johnson & Constable (1996) for original references], making them particularly suitable for TAF and PSV studies.

Table 5. Hawaiian data—VGP dispersion and mean field directions.

Volcanic Series	N_1	I_1	D_1	S_V	S_P	I_{GAD}	*Age Information (approximate)*
*Kahuka	28	21.7	8.4	13.2	17.5	35.3	10 kyr – 75 kyr
*Ninole	25	25.1	0.5	10.7	12.2	35.3	> 10 kyr
*Polulu	29	31.7	7.5	8.5	11.3	35.3	200 kyr - 300 kyr
*Kiekie	11	26.8	-7.2	8.7	13.8	38.9	0.3 Myr - 0.7 Myr
*Honolulu	25	32.1	-0.1	9.4	10.1	38.3	30 kyr - 850 kyr
^{14}C lavas	7	31.4	10.2	16.3	19.7	35.3	2.5 kyr - 17.9 kyr
Kauai	46	27.5	-3.6	13.0	14.9	38.9	3.5 Myr - 5.6 Myr
Nihoa	14	35.6	2.7	13.2	13.7	40.5	3.0 Myr
Waianae	31	34.0	-0.4	13.0	13.2	38.3	> 3.6 Myr
Brunhes data	125	27.4	3.6	12.0	12.8	37.3	
All data	216	29.1	1.5	12.8	13.3	37.3	
MMM1	238	–	–	11.0	11.8	–	
MMM2	96	–	–	11.6	12.6	–	

N_1: number of lavas in sequence. Data is described in detail in Johnson & Constable (1996).
I_1, D_1: average inclination, declination for each sequence; S_V: angular standard deviation about mean pole; S_P: angular standard deviation about geographic pole; I_{GAD}: geocentric axial dipole predicted inclination; MM1: secular variation estimate in McElhinny *et al.* (1996b), original data; MM2: secular variation estimate in McElhinny *et al.* (1996b), decimated data. Ages: these are based on information given in original references, and the full age range of a sequence may not have actually been samples in the palaeomagnetic studies. '*' denotes sequences included in the McElhinny *et al.* (1996b) study.

It is clear that the main effect of the (McElhinny *et al.* 1996b) thinning technique is to reduce the number of degrees of freedom in the data set ($N = 96$ versus $N = 238$). Adjustments to VGP dispersion estimates are noted which McElhinny *et al.* interpret as significant. However, the increase in VGP dispersion after thinning of all their data combined is mainly due to the inclusion of the Kau and Hamakua sequences (see Table 1 of McElhinny *et al.* 1996b), which display low values of S_V, correspondingly large values of S_P, and strongly biased VGP positions. Our estimates of VGP dispersion about the mean and geographic poles for all of our Brunhes data alone are very similar to the revised estimates of McElhinny *et al.*, because we do not include the data from Kau and Hamakua. Our estimates for VGP dispersion averaged over the last 5 Myr are slightly larger than those for the Brunhes alone; the data from Kauai, Nihoa and Waianae all give very consistent estimates of dispersion. With the range of our estimates of VGP dispersion, there is no apparent relationship between VGP dispersion and deviation of the mean field direction (computed for individual sequences) from that predicted by a geocentric axial dipole, suggesting no apparent relation between bias in field direction and VGP dispersion.

To confirm that our models are not affected by the type of serial correlation in directions suggested by McElhinny *et al.* (1996b), we apply their algorithm for thinning data to investigate its effect on our estimate of mean field direction. If two successive flows have mean directions which differ by less than a critical angle, ϕ, they are considered to be temporally correlated. The test is applied to successive flows until the next mean direction differs by more than ϕ from that of the initial flow. The temporally correlated flows are then averaged to form one new 'independent' observation of the field. We use the value of $\phi = 6°$, recommended by McElhinny *et al.*, and apply their thinning technique, moving first 'up' the flow sequences and then 'down' the flow sequences. These two implementations of the algorithm can yield slightly different results (Table 6) since the stratigraphic ordering of flows and initial flow in the sequence is important. [Note that our estimate of the number of independent measurements of field directions at Ninole is 11, compared with six in McElhinny *et al.* (1996b), presumably due to a different ordering of flows.] From Table 6 we can see that the mean field directions for individual sequences can change by up to 5°, but are more typically altered by less than 2°, much less than the uncertainties (α_{95}). However, the overall mean direction for all of the Hawaiian data is not altered significantly (less than 0.4°) by the thinning algorithm. The number of independent measurements is reduced from 216 to 121, effectively decreasing the signal-to-noise ratio for the Hawaiian data by 25 per cent. An inversion of our data set with the mean directions given in Table 6 and appropriate uncertainties (essentially the original uncertainties multiplied by $\sqrt{216/121}$) yields a final model virtually identical to LSN1.

Thus we have shown that the type of serial correlation discussed by McElhinny *et al.* (1996b) does not bias the estimate of the mean field direction for Hawaii, provided that volcanic sequences are available which sample different periods of the secular variation over the last 5 Myr. The central Pacific anomalies seen in our 0–5 Ma time-averaged field models are controlled primarily by large inclination anomalies, not declination anomalies, from several different Hawaiian volcanic sequences. The average inclination and declination anomalies for Hawaii for the 0–5 Myr normal polarity data are −8.2° and 1.5°, respectively. Data from 94 flows from the Mexican volcanic belt (approximately the same latitude) give an average inclination anomaly of −4.8°, and a declination anomaly of 1.7°. Thus the anomaly in the Pacific seen in the TAF models is consistent with the direct palaeomagnetic inclination observations.

Table 6. Hawaiian data—revised mean directions.

Volcanic Series	N_2	I_2	D_2	α_{95}	Δ_{12}
*Kahuka	15 (15)	21.1 (23.3)	7.3 (7.2)	6.9 (7.1)	1.0 (1.9)
*Ninole	11 (11)	22.2 (21.0)	2.4 (3.0)	8.6 (8.9)	3.2(4.7)
*Polulu	12 (13)	33.0 (32.4)	8.0 (8.0)	6.0 (5.7)	1.4 (0.8)
*Kiekie	8 (7)	28.1 (28.1)	-5.7 (-4.9)	6.8 (7.6)	1.9 (2.4)
*Honolulu	15 (17)	31.2 (31.0)	-0.5 (-0.9)	5.6 (5.2)	1.0 (1.3)
^{14}C lavas	6 (6)	29.3 (29.3)	11.1 (11.1)	16.0 (16.0)	2.2 (2.2)
Kauai	22 (21)	28.9 (28.0)	-3.5 (-3.4)	6.6 (6.7)	1.4 (0.5)
Nihoa	11 (10)	33.6 (32.2)	2.8 (2.9)	9.0 (9.4)	2.0 (3.4)
Waianae	21 (21)	33.3 (33.5)	1.3 (1.2)	5.7 (5.7)	1.6 (1.4)
All data	121 (121)	29.3 (29.1)	1.9 (2.0)	2.6 (2.6)	0.4 (0.4)

N_2: number of independent field measurements using McElhinny *et al.* (1996b) thinning method (see text). Data are decimated first moving 'up sequence', numbers in brackets indicate results obtained when data are decimated moving 'down sequence'. I_2, D_2: average inclination, declination for decimated data set; up (down) sequence. α_{95}: 95 per cent confidence cone for I_2, D_2; up (down) sequence. Δ_{12}: angle between (I_2, D_2) and (I_1, D_1); up (down) sequence. '*' denotes sequences included in the McElhinny *et al.* (1996b) study.

9 DISCUSSION

9.1 Comparison with previous time-averaged field models

A summary of the many previous studies of the time-averaged geomagnetic field is given in JC95, and a more complete review can be found in Merrill & McElhinny (1983, ch. 6 or Merrill, McElhinny & McFadden 1996, ch. 6). Most investigations have involved least-square fitting of truncated spherical harmonic expansions to sediment and/or lava-flow data sets (Merrill & McElhinny 1977; Coupland & Van der Voo, 1980; Livermore, Vine & Smith 1983; Schneider & Kent 1988, 1990; McElhinny *et al.* 1996a). With the exception of a few studies (e.g. Livermore *et al.* 1983), models derived from least-squares fitting of the data were assumed *a priori* to have zonal structure. Features common to most of these models include a large axial quadrupole term and differences between the average normal and reverse polarity fields for the last 5 Myr. The normal/reverse polarity difference has been observed in data from both lava flows and sediments (Merrill & McElhinny 1977; Merrill *et al.* 1979; review in Merrill & McElhinny 1983; Schneider & Kent 1988, 1990; Merrill *et al.* 1990), and is represented in the earlier time-averaged field models by a larger axial quadrupole term for the reverse polarity models compared with the normal polarity models. More recently McElhinny *et al.* (1966a) have used the largest currently available data set (9490 data) to construct zonal models and conclude that differences between normal and reverse polarity models are not statistically significant. Their data set contains many data which were not collected for the explicit purpose of studying second-order contributions to the geomagnetic field, and they limited their analyses to inclination anomalies averaged within 10° bands of latitude.

Other recent studies of the the time-averaged field have applied regularized inversion techniques to obtain smooth field models, whilst allowing longitudinal structure in the models (Gubbins & Kelly 1993; Carlut & Courtillot 1997; Johnson & Constable 1995; this study; Kelly & Gubbins 1997—hereafter KG97). The regularization process downweights higher-degree terms in the spherical harmonic expansion of the field, but for a given spherical harmonic degree, zonal and non-zonal terms are weighted equally. Although formal errors can be computed for the magnitudes of spherical harmonic coefficients, these are of limited value because the covariance matrix is strongly influenced by the regularization and data distribution. We compare recent published field models using maps of the radial field at the CMB. Only normal polarity field models are considered here, because of the poorer reverse polarity data distribution and concerns associated with overprinting effects. We discuss differences between our normal and reverse polarity models later. Fig. 15 shows four such normal polarity models obtained using different data sets and different modelling techniques. Figs 15(a) and (b) show two field models obtained for the average normal polarity field over the last 5 Ma, based on lava-flow data along (JC95 and KG97, respectively). The models are plotted in the Pacific Hemisphere. Fig. 15(c) shows the field model LSN1 (Fig. 11a) from this paper, and Fig. 15(d) shows a field model for the normal polarity sediment and flow data combined, but fitted to an RMS of 1.17 (iteration 19 from Fig. 9). Not shown in Fig. 15 are two other recent time-averaged field models (McElhinny *et al.* 1996a; Carlut & Courtillot 1997), although these are included in the discussions.

Two field models based on lava-flow data alone (Figs 15a and b) are similar in their long-wavelength structure, although the details of the models differ. Both models show evidence of high-latitude flux lobes in the Northern Hemisphere and similar non-zonal structure along the magnetic equator. The broad consistency between models is encouraging, since the models use different data sets, different data averaging and weighting schemes (KG97 investigate several averaging and weighting schemes; we use their 'preferred' model here), different non-linear inversion algorithms and different choices of regularization (see Table 7). Discrepancies between the two models provide a crude measure of the robustness, with respect to the choice of data and inversion procedure, of particular features in each individual field model. As mentioned in the previous section, the details of the structure in the normal polarity lava-flow models of both JC95 and KG97 are likely to be due to poorer-quality data or observations from sites

Table 7. Comparison of different time-averaged field models.

Study	*Data*	*Averaging*	*Weights*	*Algorithm*	*Regularization*
SK90	sediments only (SK90 data)	no binning	N/A	Least Squares	None
GK93, KG97	lavas only, lavas & seds (Q94 data)	no binning	regional PSV	smooth inversion(1)	Dissipation Norm
JC95	lavas only (JC96 data)	5° bins	combined PSV & within-site error	Occam	RMS B_r at CMB
This Study	lavas & seds (JC96 data) (SK90 data)	5° bins	lavas – PSV seds – 3.5°/5.0°	Occam	RMS B_r at CMB

SK90 = Schneider & Kent (1990)—modelling the data compilation; GK93 = Gubbins & Kelly (1993)—modelling; KG97 = Kelly & Gubbins (1997)—modelling; Q94 = Quidelleur *et al.* (1994)—data compilation; JC95 = Johnson & Constable (1995)—modelling; JC96 = Johnson & Constable (1996) data compilation. (1) = inversion approach described in detail in Bloxham, Gubbins & Jackson (1989)—see also Sections 7 and 9 in text.

with inferior temporal sampling. This is evident in a more recent study based on lava-flow data alone by Carlut & Courtillot (1997), who propose smoother time-averaged field models, more comparable with our LSN1 and LSR1 than with our LN1 and LR1. Carlut & Courtillot (1997) conclude, on the basis of degree and order 3 (normal polarity) or 4 (reverse polarity) inversions for the time-averaged field structure, that the only non-axial dipole term which can be estimated robustly for the time-averaged field is the axial quadrupole term.

Fig. 15(c) shows that the LSN1 field model (0–5 Ma normal polarity lava-flow and sediment data combined) is considerably smoother than the field models based on lava-flow data alone. KG97 also computed a normal polarity field model based on lava-flow and sediment data combined; in contrast to LSN1, their resulting field model was rougher than that from lava-flow data alone (Table 8; see also KG97—Table 6 and their Figs 6 and 12). The combined sediment/lava model shown in Fig. 12 of KG97 is very similar to the model we obtain by fitting our combined data set to the 95 per cent confidence limit on the $E(\chi^2)$ or a misfit level close to that of LN1 (Fig. 15d). As explained in Section 7, we believe that the combined sediment/lava data set does not have the internal consistency to warrant fitting the data to such a low RMS misfit. Thus discrepancies between LSN1 and the combined sediment/lava model of KG97 are mostly due to different prejudices about how well we should fit the data.

A potential source of confusion in comparing models presented in different studies is the estimation of uncertainty in the models. For example, KG97 present field models based on sediments/lavas combined which are considerably more complicated than ours. Although KG97 do not give an estimate of the uncertainty in these models, they do show an estimate of the formal error in their field model based on lavas alone. The errors are in general small and imply that the details of their models are significant. In contrast, our field models show less detailed structure and our estimate of uncertainty in our models is also more conservative. How can we reconcile these two sets of results? Again, the difference in the estimated uncertainties in the field models is the result of different analysis techniques. KG97 compute the formal uncertainty in their field models; they are able to do this because of the formulation of their inverse problem (they hold the damping

Table 8. Comparison of regularized models.

Study	*Model*	*Damping Parameter*	*Trace Resolution Matrix*	*RMS Misfit*	*Model Norm*
KG97	lavas only (N)	$0.5*10^{-11}$	29.5	1.02	$3.9*10^{12}$
KG97	lavas+seds (N)	$0.5*10^{-11}$	35.4	1.00	$6.4*10^{12}$
KG97	lavas+seds (R)	$0.7*10^{-11}$	27.9	1.09	$4.8*10^{12}$
JC95	lavas only (LN1)	N/A	N/A	1.21	88.6 μT
JC95	lavas only (LR1)	N/A	N/A	1.30	96.8 μT
This Study	lavas+seds (LSN1)	N/A	N/A	1.40	27.8 μT
This Study	lavas+seds (LSN1)	N/A	N/A	1.50	39.6 μT

NOTE: RMS misfits for a similar statistical fit to the data will be different for the KG97 study and this study, since the spatial binning we employ reduces the number of data in the inversions. Model norms for the two studies are different and correspond to regularization used (Table 7). Our norms are given in terms of the non-GAD RMS value for B_r at the CMB. Data for the KG97 inversions are taken from their Table 7.

parameter constant throughout the inversion and hence are able to compute resolution and covariance matrices). Our approach does not permit the estimation of the formal uncertainty in our models since the damping parameter is allowed to vary throughout the inversion. Instead we use a non-parametric estimator—the jackknife estimate of the standard error in B_r at the CMB. The formal uncertainty used by KG97 reflects mainly the effect of the spatial data distribution on the field model—the uncertainty is high where sampling of the CMB is poor. To first order, highs in the uncertainty map of KG97 (Fig. 8a) correlate with lows in our Fig. 6(b), which shows sampling of the CMB by the normal polarity lava-flow sites. Thus the overall pattern of highs and lows in the formal error maps demonstrates the extent to which the CMB is sampled, although the magnitude of the error in the field models is likely to be underestimated. In contrast, the jackknife estimate of the model error reflects the internal data consistency, and to a lesser extent the effect of site distribution. In well-sampled areas, the magnitude of the error obtained from our approach is more realistic than that of KG97.

9.2 How complex is the time-averaged field structure?

The above discussion shows that even recent results differ in the complexity required in time-averaged field models for the last 5 Ma. It is agreed that the database of palaeomagnetic directions from piston cores do not require non-zonal structure in the time-averaged field (Schneider & Kent 1990; Kelly & Gubbins 1997; this paper); disagreement stems from the level of complexity required by lava-flow data (KG97; this paper, McElhinny *et al.* 1996a; Carlut & Courtillot 1997). Our work (JC95, this paper) indicates that non-zonal structure is not only consistent with the lava-flow data, but is required to fit the observations to a reasonable level; however, others have argued that this conclusion is the result of underestimating the uncertainties in the observations (e.g. Merrill & McElhinny 1983; McElhinny *et al.* 1996a). McElhinny *et al.* (1996a) argue that both the sediment and lava-flow data sets require only an axial quadrupole term in the time-averaged field (i.e. the only signficant bias in the data from a GAD is an inclination anomaly). At the other end of the spectrum are the very complicated time-averaged field models of KG97 and models we obtain for comparable misfit levels to those of KG97.

Recent new palaeomagnetic data from several studies (e.g. data from the Azores, Iceland, Hawaii and New Zealand) do indicate that some of the data in existing databases need to be updated with more accurate estimates of TAF directions and estimates of PSV. It should be emphasized that the lava-flow database used in this study was compiled with conservative data-quality criteria. As a result we believe that it is more appropriate to evaluate existing data on a study-by-study basis, as was the goal of our original data compilation (Johnson & Constable 1996), rather than increasing all the data uncertainties so that only zonal TAF models are permitted. As we (Johnson & Constable 1995, 1996) and others (McElhinny & McFadden 1997; Carlut & Courtillot 1997) have noted, many data clearly need updating with new high-quality data collected for the explicit purpose of the types of detailed analyses presented here, and new data are required to fill gaps in the spatial data distribution.

Non-zonal structure in our field models LSN1 and LSR1 is greatest where we have good sampling of the CMB (Figs 6 and 7); in particular, the location of the Pacific anomaly is very well sampled. On the basis of the discussion in Section 7, we conclude that the additional structure in the field models of KG97 and in our previous lava-flow normal polarity model, LN1 (JC95), is the result of overfitting the data. Carlut & Courtillot (1997) also believe that some features in our previous model are poorly constrained. Carlut & Courtillot (1997) have performed extensive simulations using our code and lava-flow data sets of Quidelleur *et al.* (1994) and Johnson & Constable (1996) to investigate the influence of site distribution and data quality on the estimates of the spherical harmonic coefficients. Note that the flux lobes in the Northern Hemisphere are not observed in LSN1 (compare with LN1 and KG97), since the regularization suppresses structure in regions where data coverage is poor. It is likely that the flux lobes in the KG97 models result from overfitting the data (Figs 9 and 15).

It is apparent that current data sets incorporating palaeomagnetic directions from lava flows require non-zonal structure in the TAF to fit the data to an adequate RMS misfit (Figs 11a and b). The main non-zonal feature in the TAF is the anomaly in the radial field in the Pacific where there is good sampling of the CMB (Figs 6 and 7). The magnitude of this anomaly is not well resolved, however (Figs 11c and d), due to differences in the magnitude of the inclination anomaly associated with Pacific sediment data and lava-flow data from Hawaii. Note that if the Hawaiian anomaly reflects a crustal signal, then it must be due to induced crustal magnetization rather than to a remanent magnetization since it mostly reverses with the field. It is tempting to suppose that the anomaly is localized beneath Hawaii, because of the strong influence the Hawaiian data have on our models. However, it is important to keep in mind that the resolution achieved by these palaeomagnetic models at the CMB is very low. New data are needed throughout the Pacific to quantify the spatial extent and magnitude of the Pacific anomaly. The presence of flux lobes in the Northern Hemisphere cannot be proven, since although there is some sampling at these high latitudes, it is poor (Figs 6 and 7). The collection of high-quality, high-latitude data is needed to resolve this issue. Whilst consistent with the data, shorter-wavelength non-zonal structure in 0–5 Ma field models (e.g. LN1 of JC95 and models of KG97) is at, or beyond, the limit of the resolution of current palaeomagnetic data.

9.3 Are the normal and reverse polarity fields antipodal?

Polarity asymmetry has been the subject of much discussion over the past 20 years. Although many studies have inferred differences between normal and reverse polarity fields (Merrill & McElhinny 1977; Merrill, McElhinny & Stevenson 1979; review in Merrill & McElhinny 1983; Schneider & Kent 1988, 1990, Merrill *et al.* 1990; Johnson & Constable 1995), the dynamo equations predict antipodal normal and reverse polarity behaviour (Merrill & McElhinny 1977; Gubbins 1994). The reason for the apparent non-antipodality of the fields is not understood—suggestions include rock magnetic noise, overprinting of the reverse field, and inadequate spatial and temporal sampling. Models LSN1 and LSR1 presented here appear similar in form (Fig. 11), although LSR1 shows a greater deviation from a GAD model than LSN1 (see model norms, Table 8) as observed in the inclination and declination

anomaly data (Figs 2–4) and model predictions (Fig. 13). Fig. 15(e) shows the sum of LSN1 and LSR1, which is a measure of non-antipodality of two fields. Also shown in Fig. 15 is the standard error in model LSN1 (the better constrained of the two field models). The differences between the normal and reverse fields are seen to be insignificant relative to the uncertainties in the models themselves, especially in regions where we have good sampling of the CMB (Figs 6 and 7).

Thus, although we observe differences between normal and reverse polarities in the raw data (inclination anomalies, statistical tests of VGP latitude distributions—JC95), polarity asymmetries cannot be resolved in our field models relative to the internal consistency of the data sets. This conclusion has also been reached in recent studies by McElhinny *et al.* (1996a), based on lava and sediment data, and by Carlut & Courtillot (1997) based on lava-flow data alone. In a recent study of normal and reverse polarity data from the island of São Miguel in the Azores, we found that although the raw inclination anomaly for our reverse polarity data is greater than for our normal polarity data, the differences are not significant at the 95 per cent confidence level (Johnson *et al.* 1996). In addition, we find that biases of several degrees can be obtained even in cases where there are only slight reverse polarity overprints, particularly when low-field AF demagnetization is performed instead of thorough stepwise thermal demagnetization. As has been suggested in several other studies, such biases may well be present in a significant percentage of existing global data sets. Our results, along with other recent palaeomagnetic studies, may well shed new light on the question of polarity asymmetry.

10 CONCLUSIONS

A combined global sediment (Schneider & Kent 1990) and lava-flow (Johnson & Constable 1995, 1996) data set of palaeomagnetic directions provides improved spatial and temporal sampling of the average geomagnetic field over the period 0–5 Ma. An iterative regularized inversion algorithm designed for non-linear problems (Occam—Constable *et al.* 1987) was used to construct smooth models of the average radial field at the core–mantle boundary for normal and reverse polarity subsets of the data. The RMS misfit of the smooth normal and reverse polarity models is higher than that required to fit the data to the 95 per cent confidence limit on the expected value of chi-squared, reflecting a level of internal inconsistency of the data sets not obvious from the computed data uncertainties. Fitting the data to a lower RMS resulted in undesirable behaviour of the inversion algorithm that was not observed in previous applications (e.g. Constable *et al.* 1987; Parker 1994) and is a result of the combination of the non-linearity of our forward problem and internal inconsistencies in our data set. Non-zonal time-averaged field models (i.e. models with longitudinal structure) are required to fit the data to an acceptable level.

Our new normal (LSN1) and reverse (LSR1) polarity field models are smoother than those derived solely from lava-flow data, due to our more conservative estimates of uncertainty and the addition of a large number of lower-quality inclination-only measurements from sediment cores. However, the sampling (temporal and spatial) of these new models is much improved relative to their lava-flow-only counterparts (LN1 and LR1). Model uncertainties are also reduced. The main non-zonal feature in LSN1 and LSR1 is the anomalous radial field in the Pacific. This feature is mostly controlled by data from Hawaii—high-quality measurements from several islands—and these data should provide one of our best estimates of the time-averaged field and secular variation. There is a trade-off between spatial extent and magnitude of the anomaly, because of the quality and spatial distribution of the currently available data. Although they may be present in the average 0–5 Ma field, Northern Hemisphere flux lobes such as those seen in the historical field are beyond the resolution of the existing data set and are not seen in models LSN1 and LSR1. The non-zonal structure in both normal and reverse polarity fields is similar, suggesting the influence of long-term boundary conditions on outer core processes. The fact that the non-zonal structure reverses sign with the field would also seem to preclude crustal magnetization as the source of the structure. The reverse polarity field model shows a greater departure from an axial dipole field than the normal polarity field (as observed in many previous palaeomagnetic studies); however, the difference between the two fields is less than the uncertainties in the models. Thus, contrary to previous suggestions, normal and reverse polarity fields are not significantly different within the limits of the internal consistency of the global data set.

In summary, the time-averaged field over the last 5 Ma shows persistent non-zonal features, particularly in the Pacific Hemisphere. Differences between normal and reverse polarity fields are not significant at the resolution of the data sets. Differences in structure between recent time-averaged field models spanning the last 5 Myr (Gubbins & Kelly 1993; Johnson & Constable 1995; McElhinny *et al.* 1996a; Kelly & Gubbins 1997; Carlut & Courtillot 1997) highlight the need for new high-quality palaeomagnetic data to constrain long-term field behaviour better. Anomalous geomagnetic field behaviour coincides spatially with seismic velocity heterogeneities in the lower mantle and core–mantle boundary region (Bolton 1996; Bolton & Masters 1996; Masters *et al.* 1996; Mori & Helmberger 1995; Garnero & Helmberger 1996). The seismological observations are consistent with long-lived, long-wavelength temperature heterogeneities at the CMB beneath the central Pacific, along with the possibility of the presence of partial melt and/or localized compositional variations. We propose (Johnson & Constable 1997) that a combination of thermal and electrical conductivity heterogeneities in the lower mantle near the core–mantle boundary region may influence geomagnetic field behaviour over timescales of hundreds to millions of years. However, additional palaeomagnetic data, advances in mineral physics and progress in geodynamo modelling are needed to improve understanding of the CMB region beneath the central Pacific and to understand its effect on the geomagnetic field.

ACKNOWLEDGMENTS

We thank Harold Bolton, Lars Stixrude and Andrew Jackson for helpful discussions, Guy Masters for an early review, and Vincent Courtillot and Ron Merrill for formal reviews of the manuscript. Vincent Courtillot also previously pointed out a mistake in the appendix of our earlier paper, which led to the more accurate computation of data errors presented here. This

work was supported under NASA grant NAGW-3932 and NSF grants EAR-9526890 and EAR-9526682.

REFERENCES

Bloxham, J. & Gubbins, D., 1985. The secular variation of Earth's magnetic field, *Nature,* **317,** 777–781.

Bloxham, J., Gubbins, D. & Jackson, A., 1989. Geomagnetic secular variation, *Phil. Trans. R. Soc. Lond.,* A, **329,** 415–502.

Bloxham, J. & Jackson, A., 1990. Lateral temperature variations at the core-mantle boundary deduced from the magnetic field, *Geophys. Res. Lett.,* **17,** 1997–2000.

Bolton, H., 1996. Long period travel times and the structure of the mantle, *PhD thesis,* University of California, San Diego.

Bolton, H. & Masters, G, 1996. A region of anomalous $dlnv_s/dlnv_p$ in the deep mantle, *EOS, Trans. Am. geophys. Un.,* **77** (44), 697.

Carlut, J. & Courtillot, V., 1997, How complex is the time-averaged geomagnetic field over the last 5 million years? *Geophys. J. Int.,* submitted.

Clement, B.M., 1991. Geographic distribution of transitional VGPs: evidence for non-zonal equatorial symmetry during the Matuyama-Brunhes geomagnetic reversal, *Earth planet. Sci. Lett.,* **104,** 48–58.

Clement, B.M. & Stixrude, L., 1995. Inner core anisotropy, anomalies in the time-averaged palaeomagnetic field, and polarity transition paths, *Earth planet. Sci. Lett.,* **130,** 75–85.

Clayton, R.W. & Comer, R.P., 1983. A tomographic analysis of mantle heterogeneities from body wave travel time data, *EOS, Trans. Am. geophys. Un.,* **64,** 776.

Constable, C.G., Parker, R.L. & Stark, P.B., 1993. Geomagnetic field models incorporating frozen flux constraints, *Geophys. J. Int.,* **113,** 419–433.

Constable, S.C., Parker, R.L. & Constable, C.G., 1987. Occam's inversion: A practical algorithm for generating smooth models from electromagnetic sounding data, *Geophysics,* **52,** 289–300.

Coupland, D.H. & Van der Voo, R., 1980. Long-term nondipole components in the geomagnetic field during the last 130 Myr, *J. geophys. Res.,* **85,** 3529–3548.

Dziewonski, A.M., 1984. Mapping the lower-mantle: determination of lateral heterogeneity in P velocity up to degree and order 6, *J. geophys. Res.,* **89,** 5929–5952.

Dziewonski, A.M., 1996. Earth's mantle in three dimensions, in *Seismic Modelling of Earth Structure,* pp. 507–572, ed. Boschi, E., Ekstrom, G. and Morelli, A. Editrice composition, Bologna, Italy.

Efron, B., 1982. *The Jackknife, the Bootstrap and Other Resampling Plans,* Siam, Philadephia.

Garnero, E.J. & Helmberger, D.V., 1996. A thin laterally varying ultra-low velocity layer at the base of the mantle, *EOS, Trans. Am. geophys. Un.,* **77,** 709.

Glatzmaier, G.A. & Roberts, P.H., 1995a. A three-dimensional self-consistent computer simulation of a geomagnetic field reversal, *Nature,* **377,** 203–208.

Glatzmaier, G.A. & Roberts, P.H., 1995b. A three-dimensional convective dynamo solution with rotating and finitely conducting inner core and mantle, *Phys. Earth planet. Inter.,* **91,** 63–75.

Gubbins, D., 1988. Thermal core-mantle interactions and the time-averaged palaeomagnetic field, *J. geophys. Res.,* **93,** 3413–3420.

Gubbins, D., 1994. Geomagnetic polarity reversals: a connection with secular variation and core-mantle interaction? *Rev. Geophys.,* **32,** 61–83.

Gubbins, D. & Kelly, P., 1993. Persistent patterns in the geomagnetic field over the past 2.5 Myr, *Nature,* **365,** 829–832.

Gubbins, D. & Richards, M., 1986. Coupling of the core dynamo and mantle: thermal or topographic? *Geophys. Res. Lett.,* **13,** 1521–1524.

Gubbins, D. & Roberts, N., 1983. Use of the frozen-flux approximation in the interpretation of archaeomagnetic and palaeomagnetic data, *Geophys. J. R. astr. Soc.,* **73,** 675–687.

Hager, B. & Clayton, R., 1989. Constraints on the structure of mantle convection using seismic observations, flow models and the geoid, in *Mantle Convection,* pp. 657–763, ed. Peltier, W.R., Gordon and Breach Science Publishers, New York, NY.

Innoue, H., Fukao, Y., Tanabe, K. & Ogata, Y., 1990. Whole mantle P-wave travel time tomography, *Phys. Earth planet. Inter.,* **59,** 294–328.

Johnson, C.L. & Constable, C.G., 1995. The time-averaged geomagnetic field as recorded by lava flows over the past 5 Myr, *Geophys. J. Int.,* **122,** 489–519.

Johnson, C.L. & Constable, C.G., 1996. Paleosecular variation recorded by lava flows over the last 5 Myr, *Phil. Trans. R. Soc. Lond.,* A, **354,** 89–141.

Johnson, C.L. & Constable, C.G., 1997. Persistently anomalous pacific geomagnetic fields, *Geophys. Res. Lett.,* submitted.

Johnson, C.L., Constable, C.G., Gee, J., Staudigel, H., Tauxe, L., Salgueiro, M. & Forjaz, V.H., 1996. Paleomagnetism of 0–4 Ma lavas from São Miguel, Azores, *EOS, Trans. Am. geophys. Un.,* **77,** 165.

Jones, C., 1996. Convection driven geodynamo models. *EOS, Trans. Am. geophys. Un.,* **77,** 141.

Kelly, P. & Gubbins, D., 1997. The geomagnetic field over the past 5 Myr, *Geophys. J. Int.,* **128,** 315–330.

Kuang, W. & Bloxham, J., 1995. Numerical simulation of convective flow in a rapidly rotating spherical shell and the geodynamo, *EOS, Trans. Am. geophys. Un.,* **76,** 164.

Kuang, W. & Bloxham, J., 1996. Numerical investigations of the geodynamo, *EOS, Trans. geophys. Un.,* **77,** 141.

Li, X.-D. & Romanowicz, B., 1996. Global mantle shear-velocity model developed using nonlinear asymptotic coupling theory, *J. geophys. Res.,* **101,** 22 245–22 272.

Laj, C., Mazaud, A., Weeks, R., Fuller, M. & Herrero-Bervera, E., 1991. Geomagnetic reversal paths, *Nature,* **351,** 447.

Livermore, R.A., Vine, F.J. & Smith, A.G., 1983. Plate motions and the geomagnetic field—I. Quaternary and late Tertiary, *Geophys. J. R. astr. Soc.,* **73,** 153–171.

Loper, D.E. & Lay, T., 1995. The core-mantle boundary region, *J. geophys. Res.,* **100,** 6397–6420.

Masters, G. & Bolton, H., 1991. Large-scale shear velocity structure of the mantle, *EOS, Trans. Am. geophys. Un.,* **72,** 316.

Masters, G., Bolton, H. & Shearer, P., 1992. Large-scale 3-dimensional structure of the mantle, *EOS, Trans. Am. geophys. Un.,* **73,** 201.

Masters, G., Johnson, S., Laske, G. & Bolton, H., 1996. A shear-wave velocity model of the mantle, *Phil. Trans. R. Soc. Lond.,* **354,** 1385–1411.

McElhinny, M.W. & McFadden, P.L., 1977. Palaeosecular variation over the past 5 Myr, *Geophys. J. Int.,* submitted.

McElhinny, M.W., McFadden, P.L. & Merrill, R.T., 1996a. The time averaged paleomagnetic field 0–5 Ma, *J. geophys. Res.,* **101,** 25 007–25 027.

McElhinny, M.W., McFadden, P.L. & Merrill, R.T., 1996b. The myth of the Pacific dipole window, *Earth planet. Sci. Lett.,* **143,** 13–22.

Merrill, R.T. & McElhinny, M.W., 1977. Anomalies in the time averaged paleomagnetic field and their implications for the lower mantle, *Rev. geophys. Space Phys.,* **15,** 309–323.

Merrill, R.T. & McElhinny, M.W., 1983. *The Earth's magnetic field: its history, origin and planetary perspective,* Academic Press, London.

Merrill, R.T., McElhinny, M.W. & McFadden, P.L., 1996. *The Magnetic Field of the Earth: Paleomagnetism, the Core and the Deep Mantle,* Academic Press, San Diego, CA.

Merrill, R.T., McElhinny, M.W. & Stevenson, D.J., 1979. Evidence for long-term asymmetries in the earth's magnetic field and possible implications for dynamo theories, *Phys. Earth planet. Inter.,* **20,** 75–82.

Merrill, R.T., McFadden, P.L. & McElhinny, M.W., 1990. Paleomagnetic tomography of the core–mantle boundary, *Phys. Earth planet. Inter.,* **64,** 87–101.

Mikhlin, S.G., 1970. *Mathematical Physics, An Advanced Course,* North-Holland, London.

Miller, R.G., 1974. The jackknife—a review, *Biometrika,* **61,** 1–17.

Morelli, A. & Dziewonski, A.M., 1991. Joint determination of lateral heterogeneity and earthquake location, in *Glacial Isostacy, Sea-Level and Mantle Rheology,* pp. 514–534, ed. Sabadini, R., Lambeck, K. & Boschi, E., NATO ASI Series 334.

Mori, J. & Helmberger, D.V., 1995. Localized boundary layer below the mid-Pacific velocity anomaly identified from a PcP precursor, *J. geophys. Res.,* **100,** 20 359–20 365.

Olson, P. & Glatzmaier, G.A., 1996. Magnetoconvection and thermal coupling of the Earth's core and mantle, *Phil. Trans. R. Soc. Lond.,* A, **354,** 1413–1424.

Parker, R.L., 1994. *Geophysical Inverse Theory,* Princeton University Press, Princeton, NJ.

Prévot, M. & Camps, P., 1993. Absence of preferred longitude sectors for poles from volcanic records of geomagnetic reversals, *Nature,* **366,** 53–56.

Pulliam, R.J., Vasco, D. & Johnson, L., 1993. Tomographic inversions for mantle wave velocity structure based on the minimization of l^2 and l^1 norm of International Seismological Centre travel time residuals, *J. geophys. Res.,* **98,** 699–734.

Quidelleur, X., Valet, J-P., Courtillot, V. & Hulot, G., 1994. Long-term geometry of the geomagnetic field for the last 5 million years; an updated secular variation database from volcanic sequences, *Geophys. Res. Lett.,* **21,** 1639–1642.

Runcorn, S.K., 1992. Polar path in geomagnetic reversals, *Nature,* **356,** 654–656.

Schneider, D.A. & Kent, D.V., 1988. Inclination anomalies from Indian Ocean sediments and the possibility of a standing non-dipole field, *J. geophys. Res.,* **93,** 11 621–11 630.

Schneider, D.A. & Kent, D.V., 1990. The time-averaged palcomagnetic field, *Rev. Geophys.,* **28,** 71–96.

Su, W., Woodward, R.L. & Dziewonski, A., 1994. Degree 12 model of shear velocity heterogeneity in the mantle, *J. geophys. Res.,* **99,** 6945–6980.

Valet, J.P., Tucholka, P., Courtillot, V. & Meynadier, L., 1992. Paleomagnetic constraints on the geometry of the geomagnetic field during reversals, *Nature,* **356,** 400–407.

Vasco, D.W., Johnson, L.R. & Pulliam, J., 1995. Lateral variations in mantle velocity structure and discontinuities determined from *P, PP, S, SS,* and $SS–S_dS$ travel time residuals, *J. geophys. Res.,* **100,** 24 037–24 059.

Vasco, D.W., Pulliam, R.J., Johnson, L.R. & Earle, P.S., 1994. Robust inversions of IASP91 travel time residuals for mantle *P* and *S* velocity structure, earthquake mislocations, and station corrections, *J. geophys. Res.,* **99,** 13 727–13 755.

van der Hilst, R.D., Widiyantoro, S. & Engdahl, E.R., 1996. Evidence for deep mantle circulation from global tomography, *Nature,* **386,** 578–584.

Wilson, R.L., 1970. Permanent aspects of the earth's non-dipole magnetic field over Upper Tertiary times, *Geophys. J. R. astr. Soc.,* **19,** 417–439.

Woodward, R.L. & Masters, G., 1991. Lower mantle structure from $S_cS–S$ differential travel times, *Nature,* **352,** 231–233.

Zhang, K. & Gubbins, D., 1992. On convection in the Earth's core driven by lateral temperature variations in the lower mantle, *Geophys. J. Int.,* **108,** 247–255.